PHYSICAL REVIEW D **88,** 084009 (2013)

Generalized coherent states under deformed quantum mechanics with maximum momentum

Chee Leong Ching* and Wei Khim Ng†

Department of Physics, National University of Singapore, Kent Ridge, Singapore

(Received 25 April 2013; published 7 October 2013)

Following the Gazeau–Klauder approach, we construct generalized coherent states (GCS) as the quantum simulator to examine the deformed quantum mechanics, which exhibits an intrinsic maximum momentum. We study deformed harmonic oscillators and compute their probability distribution and entropy of states exactly. Also, a particle in an infinite potential box is studied perturbatively. In particular, unlike usual quantum mechanics, the present deformed case increases the entropy of the Planck scale quantum optical system. Furthermore, for simplicity, we obtain the modified uncertainty principle (MUP) with the perturbative treatment up to leading order. MUP turns out to increase generally. However, for certain values of γ (a parameter of GCS), it is possible that the MUP will vanish and hence will exhibit the classical characteristic. This is interpreted as the manifestation of the intrinsic high-momentum cutoff at lower momentum in a perturbative treatment. Although the GCS saturates the minimal uncertainty in a simultaneous measurement of physical position and momentum operators, thus constituting the squeezed states, complete coherency is impossible in quantum gravitational physics. The Mandel Q number is calculated, and it is shown that the statistics can be Poissonian and super-/sub-Poissonian depending on γ. The equation of motion is studied, and both Ehrenfest's theorem and the correspondence principle are recovered. Fractional revival times are obtained through the autocorrelation, and they indicate that the superposition of a classical-like subwave packet is natural in GCS. We also contrast our results with the string-motivated (Snyder) type of deformed quantum mechanics, which incorporates a minimum position uncertainty rather than a maximum momentum. With the advances of quantum optics technology, it might be possible to realize some of these distinguishing quantum-gravitational features within the domain of future experiments.

DOI: 10.1103/PhysRevD.88.084009 PACS numbers: 04.60.Bc, 03.65.−w, 04.60.−m

I. INTRODUCTION

Modified quantum mechanical commutation relations (MCRs) have been extensively studied as effective means of encoding potential gravitational or stringy effects; see Refs. [1–4] and the review [5] for a complete list of references. It has also been suggested that the consequent deformations of quantum mechanical spectra might be detectable in future low-energy experiments [3,4,6].

While most of the studied MCRs incorporate a minimum position uncertainty and usually lead to the concept of a minimal length scale [1,3,4], there are others that exhibit a maximum momentum [7–14] as in doubly special relativity (DSR). In Ref. [14], we investigated in detail large classes of deformed quantum mechanics of the latter type. The DSR-motivated MCR is exactly realized in three dimensions and is given by the commutation relation

$$[X_i, P_j] = i\hbar f_{ij}(P) = i\hbar(1 - \alpha P)\left[\delta_{ij} - \alpha \frac{P_i P_j}{P}\right] \quad (1)$$

$$[X_i, X_j] = [P_i, P_j] = 0. \quad (2)$$

Note that we have commutative geometry in this model. In one-dimensional physical subspace, the relevant modified Heisenberg quantum algebra is

$$[X, P] = i\hbar f(P), \quad (3)$$

with $f(P) = 1$ in usual quantum mechanics. The intrinsic maximum momentum arises when $f(P)$ has a singularity [13,14] or a zero at some $P = P_0$ [7–12,14]. One effect of maximum momentum is that the spectrum of bound states terminates at finite energy even for potentials like the harmonic oscillator [14]; this is in contrast to MCRs that exhibit instead a minimum position uncertainty [1,3,4].

In Ref. [14], we focused on the class of MCRs defined by

$$f(P) = 1 - 2\alpha P + q\alpha^2 P^2, \quad (4)$$

where $\alpha > 0$ and q are real parameters.[1] Indeed, α is the deformed parameter, $\alpha = \frac{\alpha_0}{M_{\rm pl}c} = \frac{\alpha_0 L_{\rm Pl}}{\hbar}$, such that $M_{\rm pl} \approx 10^{19}$ GeV$/c^2$ is the Planck mass and $L_{\rm pl} \approx 10^{-35}$ m is the Planck length. The dimensionless parameter α_0 is usually assumed to be of order unity, which implies the α-dependent terms are only important in the Planck regime, i.e., when energy and momentum are comparable to Planck energy (momentum) and the size is of the order of the Planck length. This form of MCR leads to the DSR-motivated modified uncertainty principle (MUP), which is consistent with string theory inspired generalized uncertainty principle (GUP) and results from black hole physics.

*phyccl@nus.edu.sg
†phynwk@nus.edu.sg

[1]Indeed, Eq. (4) with $q = 1$ is the one-dimensional projection of the exact three-dimensional commutation relation (1).

For $q \leq 1$, Eq. (4) has a zero, and hence (in momentum space) Eq. (3) implies an intrinsic maximum momentum. For $q > 1$, there is no intrinsic maximum momentum but rather a minimum position uncertainty. In the limits $\alpha \to 0$ and $q\alpha^2 \to \pm\beta^2$, Eq. (4) describes the Snyder (or string-motivated) [1,2] and anti-Snyder [10] algebras. The first case, with $+\beta^2$, allows for minimum position uncertainty, while the $-\beta^2$ case exhibits a maximum momentum.

The study of Eq. 3 in Ref. [14] used the momentum representation $P = p$ and $X = X(p)$, where p is the usual canonical momentum satisfying the normal Heisenberg algebra $[x, p] = i\hbar$. In Ref. [15], we discussed certain cases like a particle in a square well and scattering from a potential barrier. There, it was much easier to use the position representation $P = P(p)$ and $X = x$, where the functional form of the operator $P(p)$ can be determined exactly by Eq. (4) and the position representation of the fundamental canonical operators (x, p). In this paper, we use both the momentum and position representation interchangeably when constructing a generalized coherent state (GCS) for a particle in deformed harmonic oscillators (DHOs) and an infinite potential well.

In the next section, we review the main results of the exact energy spectrum of a particle in DHO [14] and an infinite potential well [15]. The bound states spectrum terminates at finite energy due to implicit maximum momentum. This interesting feature also manifested in the relativistic wave equation with MCR [16]. In Sec. III, we review the formalism of generalized Heisenberg algebra (GHA) [17] in constructing the so-called Gazeau–Klauder coherent states (GKCSs) [18,19].

In Sec. IV, we explicitly construct the exact GCS for $q = 1$ DHO, which is parametrized by two real and positive parameters (J, γ). Since this model exhibits maximum momentum, the general results and behaviors of the Planck length quantum optical system are different as compared to the stringy GUP case [20,21]. The entropy of the optical system turns out to increase in the presence of the maximum momentum instead of decreasing (due to the minimal length as in Ref. [20]). In Sec. V, we construct the GCS for the $q = 1$ infinite potential well using a perturbative approach. The main results are similar to the DHO case. For comparison, we investigate the anti-Snyder model for an infinite potential well, which also incorporates the maximum momentum cutoff. Since the characteristic function has the similar form as the $q = 1$ infinite potential well, we conjecture that, indeed, the increasing of entropy of any Planck length quantum optical system is the generic feature of a theory with maximum momentum cutoff, i.e., $q = 1$ MCRs and the anti-Snyder model.

In Sec. VI, for simplicity, we calculate perturbatively the MUP for $q = 1$ DHO. The MUP predicts the deviation from usual quantum mechanics in which the product of physical momentum and position uncertainties is either greater (or smaller) than $\hbar/2$, depending on γ. This scenario is in contrast to the string theory (Snyder) motivated models, whereby, in the latter case, the uncertainties are always increased due to a positive correction. This signals that GCSs saturate the minimal uncertainty in simultaneous measurement of X and P, thus behaving as a squeezed type of coherent states. However, for certain values of γ such as $\sin\gamma < 0$, it is possible for the uncertainties to vanish at certain mean energy J, which exhibits a classical characteristic. We emphasized that this result is only valid up to first-order perturbation even through phenomenologically the perturbative/approximate results are sufficient as one expects the deformed parameter alpha to be very small. We interpret these as the effects of the intrinsic high-momentum cutoff at a lower-momentum sector in a perturbative treatment. The full exact treatment with an explicit maximum-momentum cutoff shall be considered in a future study. We see that, at the quantum level, gravitational-induced uncertainty destroys complete coherency, and it is in principle impossible to have a monochromatic light ray.

Furthermore, the Mandel Q parameter can be either positive or negative with finite values of (δ, γ). This implies that the photon statistics in the GCS can be either Poissonian or super-/sub-Poissonian depending on values of γ. Thus, we can have both gravitational-induced photon bunching/antibunching effects. Ehrenfest's theorem and corresponded principle are recovered up to first order in perturbation. Fractional revival times are studied, and the revival structure is shown to be similar to the stringy case [22]. Finally, we conclude in Sec. VII.

II. MCRs WITH MAXIMUM MOMENTUM

Recall from Eqs. (3) and (4), for real momentum p, the polynomial $f(p)$ has roots at $(1 \pm \sqrt{1-q})/(\alpha q)$. Thus, for $q > 1$, the roots are away from the real line, and Eq. (3) is well defined. However, for $q = 1$, there is a doubly degenerate real root, and a momentum cutoff $P < 1/(q\alpha)$ is required. For $q < 1$, there are two real roots except at the point $q = 0$, where there is only a single real root at $1/(2\alpha)$. As we studied in Ref. [14], the position and nature of these roots determines the qualitatively different features of the deformed spectrum.

We saw that an intrinsic maximum momentum of $O(1/\alpha)$, which is favored by doubly special relativity [7], can be realized with MCRs. Defining as usual $(\Delta P)^2 = \langle P^2\rangle - \langle P\rangle^2$, it follows that, for the subclass of MCR from Eq. (4),

$$\Delta X \Delta P \geq \frac{1}{2}\langle [X, P]\rangle \geq \frac{\hbar}{2}(1 - 2\alpha\langle P\rangle + q\alpha^2\langle P^2\rangle). \quad (5)$$

This can be written as the MCR-inspired GUP:

$$\frac{2\Delta X}{\hbar} \geq \frac{(1 - \alpha\langle P\rangle)^2}{\Delta P} + \frac{(q-1)\alpha^2\langle P\rangle^2}{\Delta P} + q\alpha^2(\Delta P). \quad (6)$$

For $(q-1)>0$, the right side of Eq. (6) is positive and increases when ΔP tends to zero or infinity. Thus, there exists a subclass of the exactly realized MCRs for which ΔX has a nonzero minimum; such a minimum position uncertainty is usually associated with some fundamental length scale [5] and originally motivated the search for deformed Heisenberg algebras that would realize such scenarios [1,12]. Simply on dimensional grounds, $(\Delta X)_{\min} \sim O(\hbar\alpha)$.

As discussed in Ref. [14], $q=1$ in Eq. (4) is an exact MCR with maximum momentum cutoff $P_{\max}=1/\alpha$. For $q\neq 1$, the truncated versions of the MCRs displayed in Eq. (4), $q>1$ seems to allow for a minimum position uncertainty but no intrinsic momentum cutoff, while for $q\leq 1$, we have a maximum momentum cutoff but apparently no minimum position uncertainty.

A. MCR and DHO

The Schrodinger equation for the harmonic oscillator [14] with arbitrary q values in the momentum representation is

$$\left[\frac{p^2}{(m\hbar\omega)^2}-\left(f(p)\frac{\partial}{\partial p}\right)^2\right]\Psi(p)=\frac{2E}{m(\hbar\omega)^2}\Psi(p). \quad (7)$$

It is useful to change variables from p to a new variable ρ in such a way that the equation takes the canonical Schrodinger form. The change is defined by

$$f(p)\frac{\partial}{\partial p}\equiv\frac{\partial}{\partial\rho} \quad (8)$$

and results in the Schrodinger equation

$$\left[-\frac{\partial^2}{\partial\rho^2}+V(\rho)\right]\Psi(\rho)=\frac{2E}{m(\hbar\omega)^2}\Psi(\rho) \quad (9)$$

with positive potential

$$V(\rho)\equiv\frac{p^2(\rho)}{(m\hbar\omega)^2}. \quad (10)$$

The function $p^2(\rho)$ is determined by solving Eq. (8).

In this paper, we will focus on cases $q\leq 1$, which show the maximum intrinsic momentum cutoff $p<1/\alpha$. Particularly, $q=1$ is singled out for extra attention due to the fact that it corresponds to the exactly realized MCRs [14]. After solving the momentum function $p^2(\rho)$, the Schrodinger equation is obtained as

$$\left[-\frac{\partial^2}{\partial\rho^2}+\frac{(\rho-1)^2}{\delta^4\rho^2}\right]\Psi(\rho)=\underline{\epsilon}\Psi(\rho),\quad 0<\rho<\infty, \quad (11)$$

where the dimensionless parameters are defined as

$$\delta=\sqrt{m\hbar\omega}\alpha;\qquad \underline{\epsilon}=\frac{2E}{\hbar\omega\delta^2}. \quad (12)$$

The above equation (11) can be solved exactly, and the eigenfunctions can be obtained in terms of associated Laguerre polynomial [14,23],

$$\Psi_n^{(2a-1)}(\eta)=\sqrt{\frac{k_n n!\alpha}{(n+a)\Gamma[n+2a]}}e^{-\eta/2}\eta^a L_n^{(2a-1)}(\eta), \quad (13)$$

where

$$\eta\equiv 2k_n\rho,\qquad a\equiv\frac{1+\sqrt{1+4/\delta^4}}{2},\qquad k_n\equiv\frac{1}{\delta^4(n+a)}. \quad (14)$$

Thus, the exact (or $q=1$) MCR-corrected energy spectrum for simple harmonic oscillator (SHO) is given by

$$E_n=\frac{E_{n(0)}\sqrt{1+\frac{\delta^4}{2}}+\frac{m\alpha^2}{2}\left[(E_{n(0)})^2+\frac{(\hbar\omega)^2}{4}\right]}{\left[\sqrt{1+\frac{\delta^4}{2}}+m\alpha^2E_{n(0)}\right]^2}, \quad (15)$$

where the undeformed energy $E_{n(0)}=\hbar\omega(n+1/2)$. The energies reach $E_{\max}\leq 1/(2m\alpha^2)$ as $n\to\infty$, where we have the intrinsic maximum energy cutoff in the spectrum. For later convenience, we further define the scaled energy spectrum as

$$\tilde{\epsilon}_n=\frac{E_n}{\hbar\omega}=\frac{(n+\frac{1}{2})\left[2\sqrt{1+\frac{\delta^4}{2}}+(n+\frac{1}{2})\delta^2\right]+\frac{\delta^2}{4}}{2\left[\sqrt{1+\frac{\delta^4}{2}}+(n+\frac{1}{2})\delta^2\right]^2}. \quad (16)$$

B. MCR and free particle in a square-well potential

Considering position representation and substituting $X=x$ and $P\equiv F(p)$ in Eqs. (3) and (4) gives the differential equation

$$\frac{dF}{dp}=(1-2\alpha F+q\alpha^2F^2). \quad (17)$$

Integrating the above, we get for $q=0$

$$P=\frac{1}{2\alpha}(1-e^{-2\alpha p}) \quad (18)$$

and for $q=1$

$$P=\frac{p}{1+\alpha p}. \quad (19)$$

One can also verify by direct substitution in Eq. (3). The momentum eigenvalue equation gives

$$Pe^{ikx}=\lambda_p e^{ikx}, \quad (20)$$

which implies that $\lambda_p=\frac{1}{2\alpha}(1-e^{-2\alpha\hbar k})$ for $q=0$. Similarly for $q=1$, $\lambda_p=\frac{\hbar k}{1+\alpha\hbar k}$. Both λ_p and k are real.

Next, we use the position representation to solve exactly for the spectrum of the infinite well with walls located at $x=(0,L)$. The general plane-wave solution is given by

$$\psi(x)=Ae^{ik_1x}+Be^{ik_2x}. \quad (21)$$

Imposing the usual vanishing of the wave function at the boundaries gives the quantization condition

$$k_2 - k_1 = \frac{2n\pi}{L}, \tag{22}$$

with n an integer and the corresponding eigenfunction

$$\psi_n(x) = \frac{i}{\sqrt{2L}}(e^{ik_1x} - e^{ik_2x}). \tag{23}$$

For $q = 0$, the above expressions imply the exact energy eigenvalues

$$E_n = \frac{\pi^2\hbar^2}{2mL^2}\left[\frac{\tanh(n\tilde{\alpha})}{\tilde{\alpha}}\right]^2 (q = 0\,\text{MCR}), \tag{24}$$

where we denote the dimensionless parameter $\tilde{\alpha} = 2\pi\alpha\hbar/L$. A perturbative expansion of Eq. (24) gives

$$E_n^{\text{pert}} = \frac{n^2\pi^2\hbar^2}{2mL^2}(1 - 2n^2\tilde{\alpha}^2/3) + O(\tilde{\alpha}^4). \tag{25}$$

Similarly, for $q = 1$, the exact eigenvalues are

$$E_n = \frac{2\pi^2\hbar^2}{mL^2}\left(\frac{-1 + \sqrt{1 + (n\tilde{\alpha})^2}}{n\tilde{\alpha}^2}\right)^2 (q = 1\,\text{MCR}), \tag{26}$$

and perturbative expansion of Eq. (26) gives

$$E_n^{\text{pert}} = \frac{n^2\pi^2\hbar^2}{2mL^2}(1 - n^2\tilde{\alpha}^2/2) + O(\tilde{\alpha}^4). \tag{27}$$

Both perturbative energy (25) and (27) agree with the semiclassical expressions [14,15].

On the other hand, for the Snyder/anti-Snyder cases, it is easily shown that the exact bound state energies [15] in the infinite well are

$$E_n = \frac{\tan^2\left(\frac{\sqrt{\beta}n\pi}{L}\right)}{\beta} \quad \text{(Snyder)},$$
$$E_{n,S}^{\text{Pert}} = \frac{n^2\pi^2\hbar^2}{2mL^2}\left[1 + \frac{n^2\pi^2\hbar^2}{3mL^2}\beta\right] + O(\beta^2) \tag{28}$$

$$E_n = \frac{\tanh^2\left(\frac{\sqrt{\beta}n\pi}{L}\right)}{\beta} \quad \text{(anti-Snyder)},$$
$$E_{n,AS}^{\text{Pert}} = \frac{n^2\pi^2\hbar^2}{2mL^2}\left[1 - \frac{n^2\pi^2\hbar^2}{3mL^2}\beta\right] + O(\beta^2), \tag{29}$$

which also agree perfectly with the corresponding semiclassical results [15]. Note that the energies are limited above for the anti-Snyder case but not for the Snyder case.

III. GENERALIZED COHERENT STATES

Coherent states (CSs) were first studied by Schrodinger in 1926 in harmonic oscillator systems [24] and later by Klauder and Glauber [18,19]. Glauber obtained these states in the study of the electromagnetic correlation function and realized the interesting feature that these states saturate the Heisenberg uncertainty principle. Thus, CSs are considered quantum states with the closest behavior to the classical system and have many applications in theoretical and mathematical physics [25].

In literature, there are two ways to construct the CSs. The first is through Klauder's approach by using the Fock representation of ladder algebra, and the second is the Perelomov–Gilmore approach [26] based on group theoretic construction. In this paper, we follow Klauder's approach and use the GHA given by Ref. [17]. In this version of GHA, the Hamiltonian J_0, which is related to the characteristic function $f(x)$ of the physical system, together with ladder operators [$A^\dagger$ being creation operator and $A = (A^\dagger)^\dagger$ being the annihilation operator] play the role of the generators of the algebra,

$$J_0A^\dagger = A^\dagger f(J_0) \qquad AJ_0 = f(J_0)A$$
$$[A^\dagger, A] = J_0 - f(J_0). \tag{30}$$

We see that these operators form a closed algebra, and $f(J_0)$ is the analytic function of J_0, which is unique for each type of GHA. The Casimir of this algebra is

$$C = A^\dagger A - J_0 = AA^\dagger - f(J_0). \tag{31}$$

The vacuum of the generator J_0 is defined by

$$J_0|0\rangle = \alpha_0|0\rangle, \tag{32}$$

where α_0 is the energy eigenvalue of the vacuum state. In considering a general eigenket of J_0, denoted by $|m\rangle$, the generators satisfy

$$J_m|m\rangle = \alpha_m|0\rangle \tag{33}$$

$$A^\dagger|m\rangle = N_m|m+1\rangle \tag{34}$$

$$A|m\rangle = N_{m-1}|m-1\rangle, \tag{35}$$

where $\alpha_m = f^{(m)}(\alpha_0)$ is the mth iteration of α_0 under f and $N_m^2 = \alpha_{m+1} - \alpha_0$. In Ref. [17], it was shown that any quantum system with its eigenenergy satisfying

$$\tilde{\epsilon}_{n+1} = f(\tilde{\epsilon}_n) \tag{36}$$

fulfils the criteria of GHA. Here, $\tilde{\epsilon}_{n+1}$ and $\tilde{\epsilon}_n$ are the successive energy levels and $f(x)$ is the characteristic function of that particular quantum system. For example, one can obtain the standard harmonic oscillator with linear characteristic function $f(x) = x + 1$ and the q-deformed oscillator with $f(x) = qx + 1$. In general, GHA may not refer to the smooth deformation of Heisenberg algebra [17]. Similar to Ref. [20], we see that both the Hamiltonian of MCR-corrected DHOs and the infinite potential box are examples of those quantum systems.

Klauder's CSs are by construction the eigenstates of the family of annihilation operators,

$$A(\gamma) = e^{-i\gamma H/(\hbar\omega)}Ae^{i\gamma H/(\hbar\omega)} \tag{37}$$

$$A(\gamma)|z,\gamma\rangle = z|z,\gamma\rangle, \tag{38}$$

where $J \equiv |z|^2$ is the average energy in the elementary quantum unit of $\hbar\omega$. z is the complex eigenvalue of the annihilation operators, whereas γ is a real parameter associated with a classical action angle variable [18].

The (temporally stable) GKCSs are defined as [18]

$$|J,\gamma\rangle = \frac{1}{N(J)}\sum_{n\geq 0}\frac{J^{(n/2)}e^{-i\gamma\epsilon_n}}{\sqrt{\rho_n}}|n\rangle \tag{39}$$

$$\rho_n = \epsilon_1\epsilon_2\ldots\epsilon_n, \tag{40}$$

where we have denoted $\epsilon_n = \tilde{\epsilon}_n - \tilde{\epsilon}_0$. For consistency, we set $\rho_0 = 1$. Note that, to ensure that both (J,γ) are action angle variables, we need the GCS to satisfy

$$\langle J,\gamma|H|J,\gamma\rangle = \hbar\omega J. \tag{41}$$

We have the time independent of expectation value (temporally stable) of the Hamiltonian in the state with (J,γ).

The GCSs are said to be of Gazeau–Klauder type if they satisfy the following conditions:

(I) *normalizability:*

$$\langle J,\gamma|J,\gamma\rangle = 1, \tag{42}$$

(II) *continuity in the label:*

$$|J - J'| \to 0; \| |J,\gamma\rangle - |J',\gamma\rangle \| \to 0, \tag{43}$$

(III) *completeness:*

$$\int (d^2z) w(z,\gamma)|z,\gamma\rangle\langle z,\gamma| = 1, \tag{44}$$

where $w(z,\gamma)$ is the measure on the Hilbert space spanned by $|z,\gamma\rangle$.

The normalization constant can be expressed in terms of modified Bessel function

$$\langle J,\gamma|J,\gamma\rangle = 1 \Rightarrow N(J)^2 = \sum_{n\geq 0}^{\infty}\frac{J^n}{\rho_n}. \tag{45}$$

Strictly speaking, the GCS exists only if the radius of convergence

$$R = \lim_{n\to\infty}\sup\sqrt[n]{\rho_n} \tag{46}$$

is nonzero [19]. In fact, different choices of ρ_n and hence the characteristic function $f(\tilde{\epsilon}_n)$ give rise to many different families of GCSs. On the other hand, the temporal stability condition of the eigenstates can be obtained by

$$e^{-iHt/\hbar}|z,\gamma\rangle = |z,\gamma+\omega t\rangle. \tag{47}$$

With all the formalism discussed, we consider some examples of GCSs, namely, $q = 1$ DHO and infinite potential, as well as the Snyder/anti-Snyder case in the next section.

IV. GCS FOR MCR DEFORMED HARMONIC OSCILLATOR

In this section, we construct the GCS for the exact (or $q = 1$) MCR-deformed harmonic oscillator. Recall that from Eq. (16), the deformed energy spectra are

$$\tilde{\epsilon}_n = \frac{(n+\frac{1}{2})\left[2\sqrt{1+\frac{\delta^4}{2}} + (n+\frac{1}{2})\delta^2\right] + \frac{\delta^2}{4}}{2\left[\sqrt{1+\frac{\delta^4}{2}} + (n+\frac{1}{2})\delta^2\right]^2}.$$

From the formalism, the function ρ_n can be obtained by

$$\begin{aligned}\rho_n &:= \prod_{m=1}^{n}\epsilon_m = \prod_{m=1}^{n}\tilde{\epsilon}_m - \tilde{\epsilon}_0 \\ &= \prod_{m=1}^{n}\left[\frac{4m(4-(m-1)\delta^4 + m\delta^2\sqrt{2(2+\delta^4)})}{(\delta^2+\sqrt{2(2+\delta^4)})((2m+1)\delta^2+\sqrt{2(2+\delta^4)})^2}\right] \\ &= \frac{n!(2\mu-1)^n\mathbf{P}[2(\mu+1),n]}{\delta^{2n}(2\mu+1)^n(\mathbf{P}[\mu+\frac{3}{2},n])^2}\end{aligned} \tag{48}$$

$$\mu := \sqrt{\frac{1}{2}+\frac{1}{\delta^4}}, \tag{49}$$

where $\mathbf{P}[a,n] \equiv (\mathbf{a})_n$ is the Pochhammer symbol, which is a compact way to express the factorial

$$(\mathbf{a})_n := \frac{(a+n-1)!}{(a-1)!}; \qquad (\mathbf{a})_0 = 1. \tag{50}$$

Since we compute Eq. (48) by the exact full energy spectrum (16), we stress that it is an exact expression.[2] Thus, the exact GCS given in Eq. (39) can be written as

$$|J,\gamma\rangle = \frac{1}{N(J)}\sum_{n\geq 0}\frac{\delta^n(2\mu+1)^{n/2}\mathbf{P}[\mu+\frac{3}{2},n]J^{(n/2)}e^{-i\gamma\epsilon_n}}{(2\mu-1)^{n/2}\sqrt{n!\mathbf{P}[2(\mu+1),n]}}|n\rangle. \tag{54}$$

With the normalization condition of CS, i.e., $\langle J,\gamma|J,\gamma\rangle = 1$, we obtain the normalization constant

[2]We only manage to express the characteristic function in a closed form perturbatively. From Eq. (16), the perturbative energy up to leading order is

$$\tilde{\epsilon}_n = (n+1/2) - [3n(n+1)/2 + 1/4]\delta^2 + O(\delta^4), \tag{51}$$

and it implies that

$$\tilde{\epsilon}_{n+1} \approx \tilde{\epsilon}_n - 3(1+n)\delta^2 + 1 = \tilde{\epsilon}_n + \sqrt{1-6\delta^2\tilde{\epsilon}_n} + \frac{3}{2}\delta^2. \tag{52}$$

Hence, the characteristic function is

$$f(x) \approx x + \sqrt{1-6\delta^2 x} + \frac{3}{2}\delta^2, \tag{53}$$

which is unique for each class of GCSs.

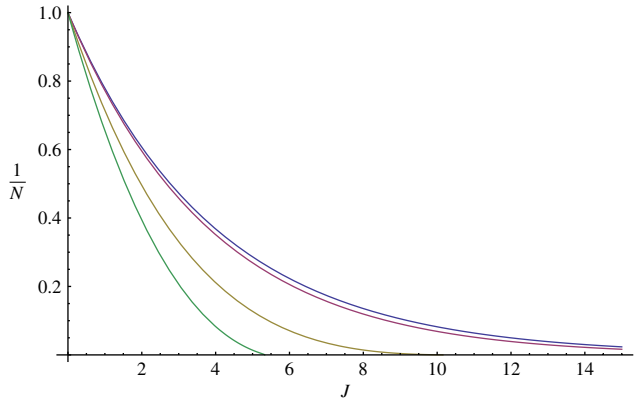

FIG. 1 (color online). The normalization factor for the $q = 1$ GCS (DHO). The blue line corresponds to $\delta = 0$. Purple, gold, and green lines are the deformed cases with $\delta = (0.1, 0.3, 0.4)$.

$$N^2(J) = {}_2\mathbf{F}_1\left[\mu + \frac{3}{2}, \mu + \frac{3}{2}; 2(\mu+1); \frac{J\delta^2(2\mu+1)}{2\mu-1}\right], \quad (55)$$

where ${}_2\mathbf{F}_1[a, b; c; d]$ is the generalized hypergeometric function. In Fig. 1, we illustrate $N^{-1}(J)$ for different values of δ. It is observed that, when $\delta \to 0$, we recover the undeformed case as $N^{-1}(J) \to e^{-J/4}$. Note that, from the phenomenological point of view, the physically acceptable range of the deformed parameter should be small, $\delta \ll 1$.

A. Probability distribution and entropy of states

Let us consider a possible aspect of Planck scale quantum optics. Indeed the GCSs we considered (39) as the states of light fields can indeed be used as an approximation to describe the real laser with a possible nonlinear interaction and a non-Poissonian statistic. Besides that, they are stable in time evolution. In standard quantum optics (i.e., $\delta = 0$), the probability of detecting n random photons is given by a Poissonian distribution [27],

$$P(n, J) = |\langle n|J\rangle|^2 = \frac{e^{-J/2}}{n!}\left(\frac{J}{2}\right)^n, \quad (56)$$

where we have previously defined $J := \langle J, \gamma|A^\dagger A|J, \gamma\rangle$ and $(\frac{J}{2})$ is the average photon number $\bar{n}$ in usual CSs. For the $q = 1$ MCR with maximum momentum,[3] the probability turns out to be

$$P(n, J, \delta) = |\langle n|J, \gamma\rangle|^2 = \frac{1}{N^2(J)}\left(\frac{J^n}{\rho_n}\right) = \frac{J^n\delta^{2n}(2\mu+1)^n(\mathbf{P}[\mu+\frac{3}{2}, n])^2(\mathbf{P}[2(\mu+1), n])^{-1}}{{}_2\mathbf{F}_1[\mu+\frac{3}{2}, \mu+\frac{3}{2}; 2(\mu+1); \frac{J\delta^2(2\mu+1)}{2\mu-1}]n!(2\mu-1)^n}. \quad (57)$$

This expression contains the physical effects of MCRs with the maximum momentum in contrast to the one with minimal length in literature, i.e., Ref. [20].

It is straightforward to show that the deformed probability distribution satisfies the normalization condition, $\sum_{n=1}^{\infty} P(n, J, \delta) = 1$. In Fig. 2, we show the overall behavior of the probability distribution $P(n, J, \delta)$ for various values of the MCR parameter. As shown, the probability distribution tends to spread out in n when δ increases. The maximum probability occurs at the $\tilde{n}$, which increases with δ and is given by the root of expression

$$\frac{J^{\tilde{n}}\delta^{2\tilde{n}}\tilde{\mu}^{-\tilde{n}}\Gamma[\mu_1+\tilde{n}]^2(H[\tilde{n}] - 2H[\mu_2+\tilde{n}] + H[\frac{\mu_1+\mu_2-3}{\tilde{\mu}}+\tilde{n}] + \ln[\frac{\tilde{\mu}}{J\delta^2}])}{{}_2\mathbf{F}_1[\mu_1, \mu_1; \mu_1+\mu_2; \frac{J\delta^2}{\tilde{\mu}}]\Gamma[\tilde{n}+1]\Gamma[\mu_1]^2\Gamma[\mu_1+\mu_2+n]} = 0, \quad (58)$$

where we have defined

$$\tilde{\mu} = \frac{2\mu-1}{2\mu+1}; \qquad \mu_1 = \frac{3}{2} + \mu; \qquad \mu_2 = \frac{1}{2} + \mu. \quad (59)$$

Here, $H[p]$ is the pth harmonic number. For fixed $J's$, the $\tilde{n}$ that gives the maximum probability increases with the MCR deformation δ.

Next, we define the Gibb entropy [28] of the system (canonical ensemble) as the standard logarithmic measure of the density of states in the phase space as

$$S(J, \delta) := -k_B \sum_{n=0}^{\infty} P(n, J, \delta) \ln P(n, J, \delta), \quad (60)$$

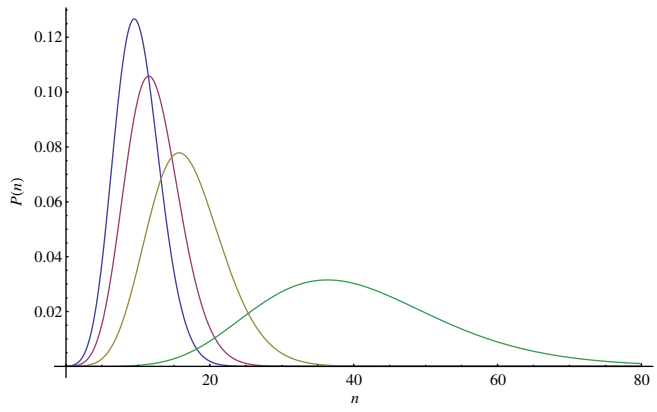

FIG. 2 (color online). The probability distribution for the $q = 1$ GCS (DHO). The blue line corresponds to $\delta = 0$. Purple, gold, and green lines are the deformed cases with $\delta = (0.1, 0.15, 0.2)$. We set $J = 20$. Notice that the peaks are shifting to larger $\tilde{n}$ as δ increases.

[3]Recall that $q \leq 1$ implicitly predicts the presence of maximum momentum, but without minimal length.

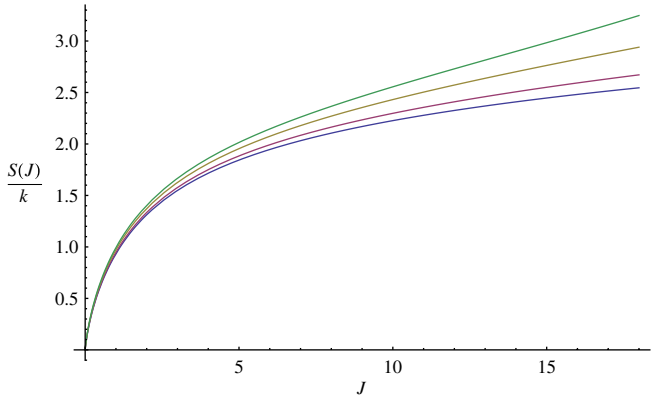

FIG. 3 (color online). The entropy distribution for the $q = 1$ GCS (DHO). The blue line corresponds to the $\delta \to 0$ limit. Purple, gold, and green lines are the deformed cases with $\delta = (0.1, 0.15, 0.18)$. Notice that the entropy is increased as δ increases.

where k_B is the Boltzmann constant. In Fig. 3, we show the plots of entropy as a function of average energy J for various values of δ. As shown, for any fixed J, the entropy increases as δ increases. It also tends to the Poissonian entropy as $\delta \to 0$, which is given by [28]

$$S^{\mathrm{Poi}}(J,0) := k_B\left[\frac{J}{2}\left(1-\ln\frac{J}{2}\right)+e^{-J/2}\sum_{n=0}^{\infty}\frac{(\frac{J}{2})^n \ln n!}{n!}\right]. \quad (61)$$

Since the entropy of the system increases with the deformation parameter and deviates from the undeformed case, it implies that the GCS tends to be "more quantum mechanical" as compared to CSs in usual quantum mechanics. As we shall see in Sec. VI, the GCSs will still saturate the modified uncertainty principle (93) but with a shifted minimum. It is consistent that both the entropy in Fig. 3 and MUP show the increasing of quantum mechanical behavior in the system considered.[4]

From another viewpoint, the MCRs we considered carry the negative modification of the effective Planck constant[5] on the right-hand side. Thus, the leading-order correction from the right-hand side of MCRs is always negative and smaller than $\hbar$. Thus, the effective size of the unit cell in the phase space decreases. This implies that the total number of accessible states and the entropy of the system increase as compared to the undeformed case. This result is different from the string theory motivated GUP case, whereby it predicts a decrease in the system's entropy due to the consequence of the minimal length scale in the theory.

[4]In Eq. (93), we see that the increasing of the MUP $(\Delta X \Delta P)^{\mathrm{mup}} > \hbar/2$ is only true for certain values of γ such as $\sin\gamma > 0$. It is possible for the MUP to vanish at a certain class of γ.

[5]This is the main difference between DSR-motivated MCRs and the string theory (Snyder) motivated GUP.

As a conclusion, these exact results are interesting because they highlight clearly some key conceptual and theoretical issues and illustrate some unique features of the MCR deformed quantum mechanics on the quantum optical behaviors.[6]

V. GCS FOR MCR DEFORMED INFINITE POTENTIAL WELL

Following the same formalism in Sec. IV, we construct the GCS for the infinite potential well perturbatively. Recall from Eq. (27) that the perturbative energy of the $q = 1$ infinite well is given by

$$\epsilon_n^{\mathrm{pert}} = \frac{n^2\pi^2\hbar^2}{2mL^2}(1 - n^2\tilde{\alpha}^2/2).$$

It implies that, up to $O(\tilde{\alpha}^2)$, we have

$$\epsilon_{n+1} = \frac{\pi^2\hbar^2}{2mL^2}(1+\tilde{\alpha}^2/2) + \frac{\sqrt{2}\pi\hbar}{\sqrt{m}L}(1-\tilde{\alpha}^2)\sqrt{\epsilon_n} + (1-3\tilde{\alpha}^2)\epsilon_n - \frac{6\sqrt{2m}\pi\hbar}{L^{5/2}}\epsilon^{3/2}, \quad (62)$$

which give us the characteristic function

$$f(x) = \frac{\pi^2\hbar^2}{2mL^2}(1+\tilde{\alpha}^2/2) + \frac{\sqrt{2}\pi\hbar}{\sqrt{m}L}(1-\tilde{\alpha}^2)\sqrt{x} + (1-3\tilde{\alpha}^2)x - \frac{6\sqrt{2m}\pi\hbar}{L^{5/2}}x^{3/2}. \quad (63)$$

The function ρ_n is found to be

$$\rho_n = \prod_{r=1}^{n}\frac{r^2\pi^2\hbar^2}{2mL^2}(1-r^2\tilde{\alpha}^2/2) = \left[-\frac{\pi^2\hbar^2}{4mL^2}\right]^n\left(\frac{\tilde{\alpha}^{2n+1}(n!)^2\Gamma[\eta_+]\Gamma[\eta_-]\sin\left(\frac{\sqrt{2}\pi}{\tilde{\alpha}}\right)}{\sqrt{2}\pi}\right), \quad (64)$$

where $\eta_\pm = n + 1 \pm \frac{\sqrt{2}}{\tilde{\alpha}}$.

Thus, the perturbative GCS for the infinite potential well is given by

$$|J,\gamma\rangle = \frac{1}{N(J)}\sum_{n\geq 0}\frac{\sqrt[4]{2}\sqrt{\pi}(\frac{2L}{\pi\hbar})^n m^{n/2}J^{(n/2)}e^{-i\gamma\epsilon_n}}{(-1)^{n/2}\tilde{\alpha}^{n+1/2}n!\sqrt{\Gamma[\eta_+]\Gamma[\eta_-]\sin\left(\frac{\sqrt{2}\pi}{\tilde{\alpha}}\right)}}|n\rangle. \quad (65)$$

From normalization condition $\langle J,\gamma|J,\gamma\rangle = 1$, we obtain the normalization constant

$$N^2(J) = {}_0\mathbf{F}_3\left[;1,\chi_-,\chi_+;-\frac{4mL^2J}{\pi^2\hbar^2\tilde{\alpha}^2}\right], \quad (66)$$

[6]Of course, to be consistent, these new features seen at high momentum need to be further verified by a relativistic treatment.

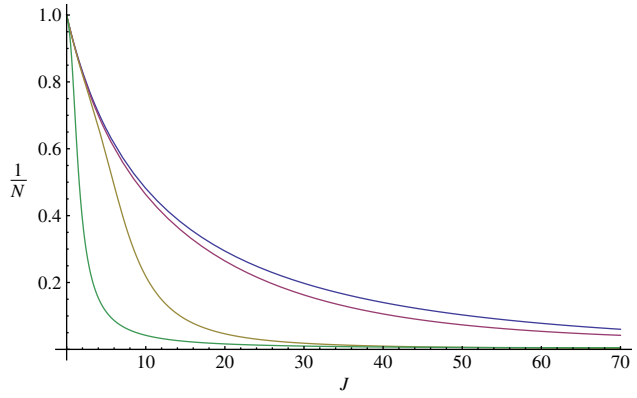

FIG. 4 (color online). The normalization factor for the $q = 1$ GCS (infinite potential well). The blue color corresponds to the $\delta \to 0$ limit. Purple, gold, and green lines are the deformed cases with $\delta = (0.035, 0.045, 0.075)$ The distribution is similar to the Fig. 1 DHO case. Here, we set $m = \hbar = L = 1$.

where again ${}_0\mathbf{F}_3[;a,b,c;d]$ is the generalized hypergeometric function and $\chi_\pm = 1 \pm \sqrt{2}/\tilde{\alpha}$. In Fig. 4, we have depicted $N^{-1}(J)$ for different values of α. Notice that the normalization function shares the same feature in both the DHO and infinite potential cases.

The probability of detecting n random photons is modified to

$$P(n,J,\delta) = \frac{1}{N^2(J)}\left(\frac{J^n}{\rho_n}\right) = \frac{(-1)^{-n}\sqrt{2}\pi(\frac{2L}{\pi\hbar})^{2n}m^n J^n}{{}_0\mathbf{F}_3[;1,\chi_-,\chi_+;-\frac{4mL^2J}{\pi^2\hbar^2\tilde{\alpha}^2}]\tilde{\alpha}^{2n+1}(n!)^2\Gamma[\eta_+]\Gamma[\eta_-]\sin(\frac{\sqrt{2}\pi}{\tilde{\alpha}})}. \tag{67}$$

From Eq. (67), the Gibb entropy of the system is given by a similar form (60). We plot the probability and generalized entropy in Figs. 5 and 6, respectively. Note that the general behaviors of the probability and entropy of the GCS infinite potential are similar compared to the DHO case.

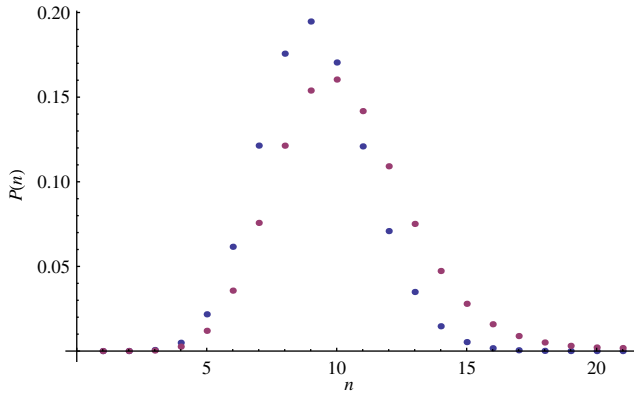

FIG. 5 (color online). The probability distribution for the $q = 1$ GCS (infinite potential well). Blue dots correspond to the $\delta \to 0$ limit. The purple dot is the deformed cases with $\delta = 0.01$. We set $J = 350$. Notice that, as in the DHO case, the peak is shifted to larger $\tilde{n}$ as δ increases.

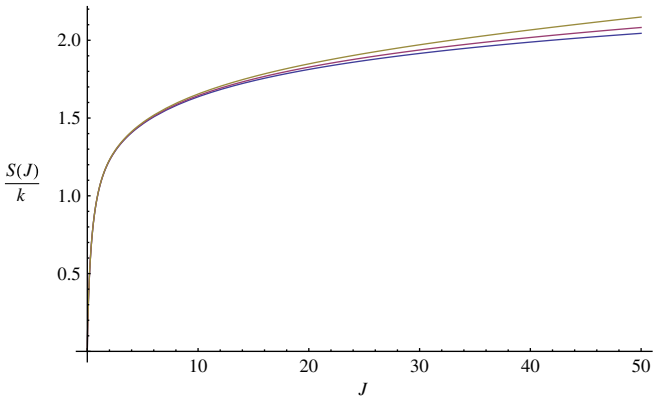

FIG. 6 (color online). The entropy distribution for the $q = 1$ GCS (infinite potential). The blue line corresponds to the $\delta \to 0$ limit. Purple and gold lines are the deformed cases with $\delta = (0.02, 0.03)$. Notice that the entropy is increased as δ increases.

To further strengthen our claim on the role of the maximum momentum cutoff in increasing the entropy of the GCS, we consider the anti-Snyder case, which also exhibits the maximum momentum. From the perturbed energy (27) and (29), it is easy to realize that the anti-Snyder case will share the same characteristic function as the $q = 1$ infinite potential case. Hence, we conclude that the anti-Snyder case gives the same physical prediction as the $q = 1$ infinite potential and DHO.

In conclusion, the increasing of entropy in the Planck scale quantum optics is the main consequence due to the maximum momentum cutoff. Evidently, this feature was obtained by the exact treatment of DHO in Sec. IV as well as the perturbative treatment in Sec. V. In addition, the probability and entropy change we obtained are opposite in sign as compared to those obtained using string theory (Snyder) motivated MCRs. Hence, these two cases are experimentally distinguishable in future experiments.

VI. UNCERTAINTY PRINCIPLES FOR DHO

To realize the deformed quantum algebra in Eq. (4) with $q = 1$, we represent the position and momentum operators from Eq. (19) perturbatively[7] up to $O(\alpha^2)$ in position space by

$$X = x; \qquad P = p(1 - \alpha p + \alpha^2 p^2), \tag{68}$$

with $[x, p] = i\hbar$ being the standard Heisenberg–Weyl algebra, and both (x, p) are canonical.[8] Here, the small letter

[7]The exact and perturbative approaches in the previous section give generic similar results.

[8]Note that we can choose an X representation for $q \leq 1$ because in this sector we have maximum momentum cutoff and no minimal length uncertainty [14], the eigenstate of physical position operator X is well-defined. We have commutative space $[x_i, x_j] = [p_i, p_j] = 0$.

p can be physically interpreted as the momentum operator at low energies and thus carries the standard representation in position space, i.e., $p = \frac{\hbar}{i}\frac{\partial}{\partial x}$. It is very important to note that, since we represent the deformed momentum operator perturbatively (68), the results in this and subsequent sections will be interpreted as the effects and manifestations of the intrinsic high-momentum cutoff at lower momentum in a perturbative treatment.

With Eq. (68), any (nonrelativistic) quantum mechanical Hamiltonian is modified to

$$\begin{aligned} H(X,P) &= \frac{P^2}{2m} + V(X) \\ &= \left[\frac{p^2}{2m} - \frac{\alpha}{m}p^3 + \frac{3\alpha^2}{2m}p^4 + O(\alpha^3)\right] + V(x) \\ &= H_0 + H_1, \end{aligned} \tag{69}$$

where the undeformed Hamiltonian $H_0 = \frac{p^2}{2m} + V(x)$ and perturbed Hamiltonian $H_1 = -\frac{\alpha}{m}p^3 + \frac{3\alpha^2}{2m}p^4 + O(\alpha^3)$. For harmonic potential, we have

$$H(X,P)|_{\mathrm{DHO}} = \left[\frac{p^2}{2m} + \frac{m\omega^2 x^2}{2} - \frac{\alpha p^3}{m} + \frac{3\alpha^2}{2m}p^4\right], \tag{70}$$

where we ignore the higher-order terms. Next, we introduce the canonical creation-annihilation operators,

$$A := \sqrt{\frac{m\omega}{2\hbar}}\left(x + \frac{ip}{m\omega}\right), \qquad A^\dagger := \sqrt{\frac{m\omega}{2\hbar}}\left(x - \frac{ip}{m\omega}\right). \tag{71}$$

They satisfy the canonical commutation relations,

$$[A, A^\dagger] = 1 \qquad [A, A] = [A^\dagger, A^\dagger] = 0. \tag{72}$$

The standard Fock basis of SHO is given by

$$\begin{aligned} &A|0\rangle = 0, \qquad A|n^{(0)}\rangle = \sqrt{n}|n^{(0)} - 1\rangle, \\ &A^\dagger|n^{(0)}\rangle = \sqrt{n+1}|n^{(0)} + 1\rangle. \end{aligned} \tag{73}$$

The perturbative Hamiltonian of DHO turns out to be

$$\begin{aligned} H = \hbar\omega\Bigg[&\left(N + \frac{1}{2}\right) + i\frac{\alpha\sqrt{m\hbar\omega}}{2^{3/2}}(A^\dagger - A)^3 \\ &+ \frac{3m\hbar\omega\alpha^2}{8}(A^\dagger - A)^4\Bigg], \end{aligned} \tag{74}$$

where $N = A^\dagger A$ is the number operator. The perturbative energy spectrum is given by

$$\tilde{\epsilon}_n = \left(n + \frac{1}{2}\right) - \frac{3}{2}n(n+1)\delta^2 - \frac{\delta^2}{4}; \quad \delta = \sqrt{m\hbar\omega}\alpha \tag{75}$$

$$\Rightarrow \epsilon_n = \tilde{\epsilon}_n - \tilde{\epsilon}_0 = n\left[1 - \frac{3}{2}(n+1)\delta^2 + O(\alpha^4)\right], \tag{76}$$

which is consistent with the expansion of the exact energy spectrum in Eq. (16). Using the identity

$$\frac{\Gamma(2 - \frac{2}{3\delta^2})}{\Gamma(n + 2 - \frac{2}{3\delta^2})} = \left(\frac{-3\delta^2}{2}\right)^n\left[1 + \frac{3n(n+3)\delta^2}{4} + O(\delta^4)\right], \tag{77}$$

we obtain the perturbative normalization constant as

$$N(J) = \exp[J/2]\sqrt{\left(1 + \frac{3J(J+4)}{4}\delta^2 + O(\delta^4)\right)}. \tag{78}$$

The GCS in the perturbative setting is expressed as

$$|J,\gamma\rangle = \sum_{n\geq 0}\frac{[1 + \frac{1}{8}(6n(n+3) - 3J(J+4))\delta^2]J^{(n/2)}e^{-i\gamma\epsilon_n}}{\sqrt{n!}}|n\rangle. \tag{79}$$

The deformed number states can be expanded in terms of the undeformed one by the standard Rayleigh–Schrodinger perturbation theory, in which, up to first order, we have[9]

$$\begin{aligned} |n\rangle &= |n^{(0)}\rangle + \sum_{k\neq n}^{\infty}\frac{\langle k^{(0)}|H_1|n^{(0)}\rangle}{\epsilon_n^0 - \epsilon_k^0}|k^0\rangle \\ &= |n^{(0)}\rangle + i\frac{\delta}{\sqrt{8}}\Bigg[\left(-\frac{1}{3}\right)\left(\sqrt{(n+1)_3}|n^{(0)} + 3\rangle\right. \\ &\quad \left. + \sqrt{(n-2)_2}|n^{(0)} - 3\rangle\right) + 3\left(\sqrt{(n+1)_3}|n^{(0)} + 1\rangle \right. \\ &\quad \left. + \sqrt{(n)_3}|n^{(0)} - 1\rangle\right)\Bigg]. \end{aligned} \tag{80}$$

Note that $(a)_n$ is the Pochhammer symbol defined in Eq. (50).

Also, the (perturbative) physical position and momentum operator can be further expressed in terms of creation/annihilation operators as

$$X = x = \sqrt{\frac{\hbar}{2m\omega}}[A^\dagger + A] \tag{81}$$

$$X^2 = x^2 = \frac{\hbar}{2m\omega}[(A^\dagger)^2 + A^2 + 2N + 1] \tag{82}$$

[9]Phenomenologically, the perturbative results are sufficient, as one expects alpha to be very small. So, we shall keep up to $O(\alpha)$ terms consistently in the subsequent section.

$$P = p - \alpha p^2 + O(\alpha^2) = \sqrt{\frac{m\hbar\omega}{2}}\left[i(A^\dagger - A) + \frac{\delta}{\sqrt{2}}[(A^\dagger)^2 + A^2 - 2N - 1] + O(\delta^2) \right]$$
$$P^2 = p^2 - 2\alpha p^3 + O(\alpha^2) = \frac{m\hbar\omega}{2}\{-[(A^\dagger)^2 + A^2 - 2N - 1] + i\sqrt{2}\delta[(A^\dagger)^3 - A^3 + 3[A^\dagger A^2 - (A^\dagger)^2 A + A - A^\dagger]] + O(\delta^2)\}. \tag{83}$$

Next, we compute the position and momentum dispersion for the perturbative GCS in Eq. (79). After a lengthy but straightforward calculation,[10] we obtain

$$\langle X\rangle = \sqrt{\frac{\hbar}{2m\omega}}[\langle A^\dagger\rangle + \langle A\rangle] = \sqrt{\frac{2\hbar J}{m\omega}}[\cos\gamma + \delta\sqrt{2J}\sin(2\gamma) + O(\delta^2)] \tag{84}$$

and also

$$\langle X^2\rangle = \frac{\hbar}{2m\omega}[\langle (A^\dagger)^2\rangle + \langle A^2\rangle + 2\langle N\rangle + 1] \tag{85}$$

$$= \frac{\hbar}{2m\omega}[1 + 2J(\cos 2\gamma + 1) + 4\sqrt{2J}\delta[(J+1)\sin\gamma + J\sin 3\gamma] + O(\delta^2)]. \tag{86}$$

Using the standard interpretation of uncertainty as standard deviation $(\Delta X) = \sqrt{\langle X^2\rangle - \langle X\rangle^2}$, the MCRs dispersion in position operator X is

$$\frac{(\Delta X)^{\mathrm{mcr}}}{(\Delta X)^{qm}} = 1 + 2\sqrt{2J}\delta\sin\gamma + O(\delta^2), \tag{87}$$

whereby we denote $(\Delta X)^{qm} = \sqrt{\hbar/(2m\omega)}$. We see that Eq. (87) recovers the standard undeformed result when $(\Delta X)^{\mathrm{mcr}}_{\delta\to 0} = \sqrt{\hbar/(2m\omega)}$. Also, for the special case when $\gamma = 0$, we have the same minimal position uncertainty $(\Delta X)^{\mathrm{mcr}}_{\gamma\to 0} = (\Delta X)^{qm}$. In general, for any finite J and nonzero parameters ($\delta \neq 0$, $\gamma \neq 0$), the position dispersion $(\Delta X)^{\mathrm{mcr}}$ can either increase or decrease as compared to $\sqrt{\hbar/(2m\omega)}$, depending on the values of γ. It implies that, although GCSs saturate the position uncertainty as in standard CSs, the absolute minimum is shifted with the deformed parameter δ and γ. Similar to Eq. (87), the string theory motivated GUP position uncertainty is given by [22]

$$\frac{(\Delta X)^{\mathrm{gup}}}{(\Delta X)^{qm}} = 1 + \frac{m\hbar\omega\beta}{2}(1 + J(2 - 2\gamma\sin 2\gamma - \cos 2\gamma)) + O(\beta^2), \tag{88}$$

where β is the deformed parameter proportional to L_{pl}^2 and has the dimension of an inverse squared momentum. Similar to our MCR case, this position uncertainty can take both positive and negative corrections.

[10] See the Appendix for a more detailed calculation.

With the same token, the momentum expectation value in $|J, \gamma\rangle$ is

$$\frac{\langle P\rangle}{\sqrt{m\hbar\omega}} = -\sqrt{2J}\sin\gamma + \delta(1 + 2J(1 + \cos 2\gamma)) + O(\delta^2), \tag{89}$$

and

$$\frac{2\langle P^2\rangle}{m\hbar\omega} = 1 + 2J(1 - \cos\gamma) - 4\sqrt{2J}\delta(J\sin 3\gamma + (J+1)\sin\gamma) + O(\delta^2). \tag{90}$$

The MCRs dispersion in momentum operator P is

$$\frac{(\Delta P)^{\mathrm{mcr}}}{(\Delta P)^{qm}} = 1 + O(\delta^2), \tag{91}$$

whereby we denote $(\Delta P)^{qm} = \sqrt{\frac{m\hbar\omega}{2}}$. From Eq. (91) we see that the deformed momentum uncertainty is similar to the standard CS up to the first-order perturbation, regardless of values for (J, γ).

The stringy momentum dispersion is given by [22]

$$\frac{(\Delta P)^{\mathrm{gup}}}{(\Delta P)^{qm}} = 1 - \frac{m\hbar\omega\beta J}{2}(\cos 2\gamma - 2\gamma\sin 2\gamma). \tag{92}$$

We see that stringy momentum uncertainty (92) can increase or decrease as compared to the undeformed case, depending on the values of γ. For our MCR case (91), it is always unchanged with respect to (J, γ). We see from Eqs. (88) and (92) that the GUP position and momentum uncertainties are behaving like the conjugate pair for all finite values of J and β, but not in the MCR case since $(\Delta P)^{\mathrm{mcr}}$ is always constant up to the leading order in perturbation.

The product of both position and momentum uncertainties for the MCR produces the MUP,

$$\left[\frac{\Delta X\Delta P}{\hbar/2}\right]^{\mathrm{mup}} = 1 + 2\sqrt{2J}\delta\sin\gamma + O(\delta^2) = 1 - 2\alpha\langle J, \gamma|P|J, \gamma\rangle + O(\delta^2). \tag{93}$$

For comparison, the stringy GUP is given by [21]

$$\left[\frac{\Delta X\Delta P}{\hbar/2}\right]^{\mathrm{gup}} = 1 + \frac{1}{2}\beta m\hbar\omega(1 + 4J\sin^2\gamma) + O(\beta^2) = 1 + \beta\langle J, \gamma|P^2|J, \gamma\rangle + O(\beta^2). \tag{94}$$

First, both Eqs. (93) and (94) produce the correct undeformed limit. Let us consider the special case when

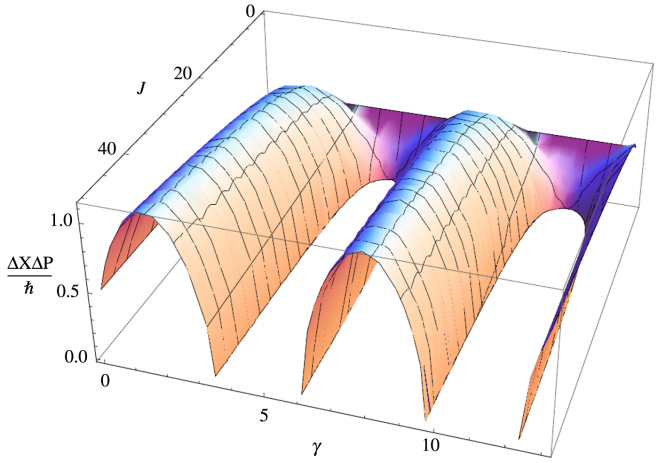

FIG. 7 (color online). The MUP. We set $\delta = 0.1$. The edge of the plot with $J \neq 0$; $\gamma \neq 0$ carries the vanishing uncertainty principle $\Delta X \Delta P = 0$.

$\gamma = 0$; we have $[(\Delta X)(\Delta P)]^{\text{mup}}_{\gamma=0} = \hbar/2$ for MUP and $[(\Delta X)(\Delta P)]^{\text{gup}}_{\gamma=0} = \hbar\sqrt{1 + \frac{1}{2}\beta m\hbar\omega J}$ for the GUP. Thus, in deformed quantum theory, the MCR predicts no change in the uncertainty principle for the GCS when $\gamma = 0$. This scenario is effectively different from the GUP. The latter implies an increase in the uncertainty principle for all finite values of β.

However, for nonzero γ, the situation is drastically different from $\gamma = 0$. In Fig. 7, for some finite values of γ, the product uncertainties of position and momentum operators vanish, i.e., $[(\Delta X)(\Delta P)]^{\text{mup}} = 0$, which exhibits the classical characteristic[11] as in the MCR-deformed SHO [14]. The stringy GCS always further increases the minimal uncertainty in the product of $(\Delta X)(\Delta P)$. This feature can be the empirical significance to distinguish between the MCR and GUP schemes of quantum deformation besides the entropy in Sec. IV.

The energy of the MCR-deformed GCS (without zero point energy) turns out to be

$$\langle J, \gamma|H|J, \gamma\rangle = \langle J, \gamma|\left(\frac{P^2}{2m} + \frac{m\omega^2 X^2}{2m} - \frac{\hbar\omega}{2}\right)|J, \gamma\rangle. = \hbar\omega J. \tag{95}$$

Equation (95) is the consistency condition to ensure that the energy behaves as the action angle variable, and GCSs remain coherent states under time evolution (temporally stable).

[11]The existence of such classical phase, i.e., $(\Delta X)(\Delta P)]^{\text{mup}} = 0$, is fundamentally different in physical grounds from the one in Ref. [14]. For the latter, the vanishing of the uncertainty principle is directly due to the intrinsic maximum momentum cutoff. In fact, at the maximum momentum state ($n_{\max} \to \infty$ for $q = 1$), the right-hand side of the MCR (4) vanishes. For the GCS, the uncertainties vanish for certain classes of γ (action angle variable).

A. Quantum statistic of coherent state

One can further compute the dispersion of the number operator $N = A^\dagger A$. First, up to first order in perturbation $O(\delta)$, we have the following expectation values[12]:

$$\langle J, \gamma|A^\dagger A|J, \gamma\rangle = J\left[1 + \frac{\delta}{\sqrt{2J}}(J\sin 3\gamma - 3(J+1)\sin\gamma)\right] \tag{96}$$

$$\langle J, \gamma|(A^\dagger)^2 A^2|J, \gamma\rangle = J^2\left[1 + \sqrt{\frac{2}{J}}\delta((J+1)\sin 3\gamma - 3(J+2)\sin\gamma)\right] \tag{97}$$

The respective expectation values of N and N^2 are given by

$$\langle J, \gamma|N|J, \gamma\rangle = \langle J, \gamma|A^\dagger A|J, \gamma\rangle = J\left[1 + \frac{\delta}{\sqrt{2J}}(J\sin 3\gamma - 3(J+1)\sin\gamma)\right] \tag{98}$$

$$\langle J, \gamma|N^2|J, \gamma\rangle = \langle J, \gamma|(A^\dagger)^2 A^2|J, \gamma\rangle + \langle J, \gamma|A^\dagger A|J, \gamma\rangle = J(J+1) + \sqrt{\frac{J}{2}}\delta\sin\gamma[2J(2J+3)\cos 2\gamma - 4J(J+3) - 3]. \tag{99}$$

The dispersion of the number operator turns out to be

$$\langle J, \gamma|(\Delta N)^2|J, \gamma\rangle = \langle J, \gamma|N^2|J, \gamma\rangle - (\langle J, \gamma|N|J, \gamma\rangle)^2 = J\left[1 + \frac{3\delta\sin\gamma}{\sqrt{2J}}(2J(\cos 2\gamma - 1) - 1) + O(\delta^2)\right]. \tag{100}$$

In quantum optics, the measure of deviation from the standard Poissonian distribution is given by the Mandel parameter, defined by [27]

$$Q := \frac{\langle J, \gamma|(\Delta N)^2|J, \gamma\rangle}{\langle J, \gamma|N|J, \gamma\rangle} - 1, \tag{101}$$

where $Q = 0$ refers to standard Poissonian distribution, $Q \geq 0$ the super-Poissonian (photon bunching), and $Q \leq 0$ the sub-Poissonian (photon antibunching). Thus, for GCSs of DHO, we have

$$Q = \frac{1 + \frac{3\delta\sin\gamma}{\sqrt{2J}}(2J(\cos 2\gamma - 1) - 1)}{1 + \frac{\delta}{\sqrt{2J}}(J\sin 3\gamma - 3(J+1)\sin\gamma)} - 1 = -4\sqrt{2J}\delta\sin^3\gamma + O(\delta^2). \tag{102}$$

The CS, the output by a laser far above threshold, has Poissonian statistics yielding random photon spacing. However, from Eq. (102), we see that the GCS no longer

[12]Refer to Appendix for more details.

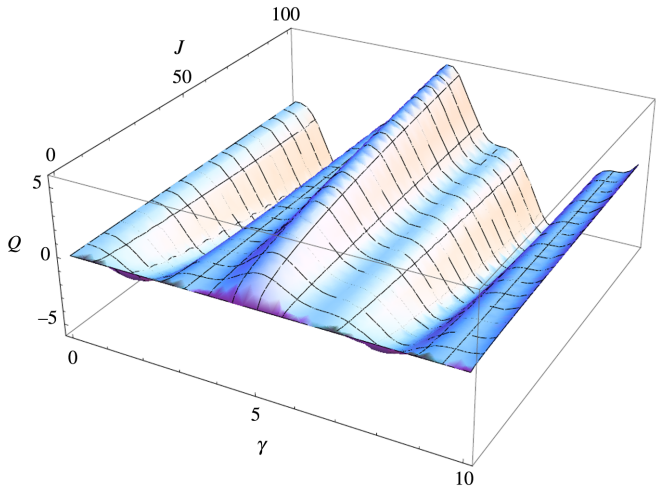

FIG. 8 (color online). The Mandel Q number for the GCS. We set $\delta = 0.1$. Note that the Mandel Q number can be positive or negative periodically depending on the parameter γ.

purely exhibits random Poissonian distribution. The effect of Eq. (102) can be considered as the MCR gravitational induced super-/sub-Poissonian statistics. Thus, within the framework of GCS, photons can arrive either more (positively correlated) or less (negatively correlated) simultaneously at the detectors depending on the value of γ. In Fig. 8, we show that the variation of the Mandel Q number as a function of γ. We have the sub-Poissonian case when $\gamma \in (0, \pi) + 2r\pi$ and super-Poissonian case when $\gamma \in (\pi, 2\pi) + 2r\pi$, where r is any positive integers. In contrast to Eq. (102), the stringy motivated GUP predicts the sub-Poissonian distribution for the GCS regardless of (β, γ).

B. Semiclassical dynamics

We consider the dynamics of DHO in the framework of the MCR that incorporates the maximum momentum by using the Heisenberg picture. To quantify how closely our GCSs resemble classical mechanics, we can test Ehrenfest's theorem. For any bounded operator O, the theorem is given by

$$\frac{d}{dt}\langle J, \gamma + t\omega|O|J, \gamma + t\omega\rangle = \frac{i}{\hbar}\langle J, \gamma + t\omega|[H, O]|J, \gamma + t\omega\rangle, \tag{103}$$

where $|J, \gamma + t\omega\rangle$ is the time evolution of states $|J, \gamma\rangle$ under the Hamiltonian such that $|J, \gamma + t\omega\rangle = \exp(-iHt/\hbar)|J, \gamma\rangle$. Using the deformed Hamiltonian, the Heisenberg equation of motion (EOM) for the position of the center of the wave packet takes the form of

$$\begin{aligned}\langle J, \hat{\gamma}|\dot{X}|J, \hat{\gamma}\rangle &= \frac{i}{\hbar}\langle J, \hat{\gamma}|[H, X]|J, \hat{\gamma}\rangle = i\sqrt{\frac{\hbar\omega}{2m}}\left[\langle [A^\dagger A, (A^\dagger + A)]\rangle + \frac{i\delta}{2\sqrt{2}}\langle [(A^\dagger - A)^3, (A^\dagger + A)]\rangle + O(\delta^2)\right] \\ &= i\sqrt{\frac{\hbar\omega}{2m}}\left[\langle A^\dagger\rangle - \langle A\rangle + \frac{3i\delta}{\sqrt{2}}(2\langle A^\dagger A\rangle - \langle (A^\dagger)^2\rangle - \langle A^2\rangle + 1) + O(\delta^2)\right] \\ \Rightarrow m\langle J, \hat{\gamma}|\dot{X}|J, \hat{\gamma}\rangle &= \sqrt{m\hbar\omega}[-\sqrt{2J}\sin\hat{\gamma} + 4J\delta\cos 2\hat{\gamma} + O(\delta^2)],\end{aligned} \tag{104}$$

where we have denoted $\hat{\gamma} := \gamma + t\omega$. We see that, by taking time derivative of Eq. (84) and comparing it to Eq. (104), one can obtain the Ehrenfest theorem. Also, by taking limit $\delta \to 0$, we recover the exact Ehrenfest theorem for usual quantum mechanics. With the same token, the EOM of the momentum operator is

$$\begin{aligned}\langle J, \hat{\gamma}|\dot{P}|J, \hat{\gamma}\rangle &= \frac{i}{\hbar}\langle J, \hat{\gamma}|[H, P]|J, \hat{\gamma}\rangle = i\sqrt{\frac{m\hbar\omega^3}{2}}[i\langle [A^\dagger A, (A^\dagger - A)]\rangle + \sqrt{2}\delta\langle [A^\dagger A, (A^\dagger - A)^2]\rangle + O(\delta^2)] \\ &= i\sqrt{\frac{m\hbar\omega^3}{2}}[i(\langle A^\dagger\rangle + \langle A\rangle) + \sqrt{2}\delta(\langle (A^\dagger)^2\rangle - \langle A^2\rangle)\rangle + O(\delta^2)] \\ &= -\sqrt{2m\hbar J\omega^3}\cos\hat{\gamma} - 4J\sqrt{m\hbar\omega^3}\delta\sin 2\hat{\gamma} + O(\delta^2).\end{aligned} \tag{105}$$

By taking time derivative of Eq. (89), we are in complete agreement with Eq. (105). It is worth noticing that, in the stringy motivated model, this requirement is not exactly satisfied by the authors in Ref. [21] but further rectified by the author in Ref. [22] by applying the non-Hermitian quantum mechanics approach.

Next, we differentiate Eq. (104) and use Eq. (84) in order to obtain the deformed Newton EOM,

$$\begin{aligned}\langle J, \hat{\gamma}|\ddot{X}|J, \hat{\gamma}\rangle &= -\omega^2\left[\sqrt{\frac{2\hbar J}{m\omega}}\cos\hat{\gamma} + 8J\delta\sqrt{\frac{\hbar}{m\omega}}\sin 2\hat{\gamma}\right] \\ &= -\omega^2\left[\langle J, \hat{\gamma}|X - \frac{3\delta}{\sqrt{m\hbar\omega}}(XP + PX)|J, \hat{\gamma}\rangle\right].\end{aligned} \tag{106}$$

Note that the correspondence principle in the MCR-deformed quantum theory is modified, and generally the center of the wave packet no longer follows the DHO path. Interestingly, we produce the similar correspondence principle as in the stringy case [22]. Indeed, the classical dynamics of the GCS is not strictly simple harmonic.

Next, we consider

$$\left\langle -\frac{\partial V}{\partial x}\right\rangle = -m\omega^2\langle X\rangle = -\sqrt{2m\hbar J\omega^3}[\cos\hat{\gamma} + \sqrt{2J}\delta\sin 2\hat{\gamma}]. \quad (107)$$

Comparing with Eq. (105), the Ehrenfest theorem is satisfied perturbatively, and it is given by $\langle\dot{P}\rangle = \langle -\frac{\partial V}{\partial x}\rangle$ for arbitrary values of γ.

C. Fractional revival times

In this section, we study the revival structure of the GCS wave packet under MCR-deformed quantum theory. It is commonly known that, when a wave function evolves in time to a state that closely resembles its initial form, we have the quantum revival phenomena. In addition, fractional revival occurs in a situation when a wave function evolves in time to another state that can be described as a collection of spatially distributed subwave functions, each of which closely resembles the shape of the initial wave function [18].

The wave packet in our GCS can be written as[13]

$$|J, \omega t\rangle = \sum_{n=0}^{\infty} c_n(J)e^{-i\epsilon_n t/\hbar}|n\rangle, \quad (108)$$

with normalization condition $\sum_{n\geq 0}|c_n(J)|^2 = 1$. The weighting probabilities $|c_n(J)|^2$ are defined by $c_n(J) := J^{n/2}/N(J)\sqrt{\rho_n}$. The revival phenomena arise from the weighting probabilities in the way that it describes well-localized behavior of the wave packet under sub-(super-) Poissonian distribution. In Ref. [18], one can expand the energy in the expression for wave packets around the centrally excited submode $\tilde{n}$, with energy $E_{\tilde{n}}$. This submode refers to the peak of $|c_n(J)|^2$ in which it is governed by corresponding distributions. The submode is assumed to be close to the expectation value of the number operator $\tilde{n} \approx \bar{n} = \langle N\rangle = Jd\ln N^2(J)/dJ$. The revival time scales are given by the derivatives of the energy, i.e., classical period $T_{cl} = 2\pi\hbar/|\epsilon'_{\tilde{n}}|$, revival time $T_{\rm rev} = 4\pi\hbar/|\epsilon''_{\tilde{n}}|$, super-revival time $T_{\rm srev} = 12\pi\hbar/|\epsilon'''_{\tilde{n}}|$, and so on. Note that the energy of our system is quadratic in n, and thus we only have nonzero classical period $T_{\rm cl}$ and revival time $T_{\rm rev}$ for the system.

Now, consider the $q = 1$ MCR-deformed harmonic oscillator. We treat it perturbatively up to the leading-order correction. Considering the perturbative energy spectra (76), the deformed probability density (and its inverse) to leading order is

$$\rho_n = \frac{(-\frac{3}{2})^n\delta^{2n}n!\Gamma(n+2-2/(3\delta^2))}{\Gamma(2-2/(3\delta^2))} + O(\delta^2) \quad (109)$$

$$\Rightarrow \frac{1}{\rho_n} = \frac{1}{n!} + \frac{3(n+3)\delta^2}{4(n-1)!} + O(\delta^4). \quad (110)$$

The normalization constant and the weighting function are given by

$$N^2(J) := \sum_{n=0}^{\infty}\frac{J^n}{\rho_n} \approx e^J\left[1 + \frac{3J}{4}(J+4)\delta^2\right] \quad (111)$$

$$|c_n(J)|^2 := \frac{J^n(\frac{1}{n!} + \frac{3(n+3)\delta^2}{4(n-1)!})}{e^J(1+\frac{3J}{4}(J+4)\delta^2)} \approx \frac{J^ne^{-J}}{n!}\left[1 - \frac{3[J(J+4) - n(n+3)]\delta^2}{4}\right]. \quad (112)$$

In Eq. (112), we see that the usual Poissonian weighting function $|c_n^{\rm poi}(J)|^2 = J^ne^{-J}/n!$ is modified due to the deformation. In fact, Eq. (112) is the perturbative expansion of the exact probability density in Eq. (57). In Fig. 9, we plot the modified weighting function for various energy J as the functions of n. Note that the peak refers to the dominating submode $\tilde{n}$. This submode is given by

$$\tilde{n} \approx \langle J, \gamma|N|J, \gamma\rangle = J\left[1 + \frac{\delta}{\sqrt{2J}}(J\sin 3\gamma - 3(J+1)\sin\gamma) + O(\delta^2)\right]. \quad (113)$$

Besides that, the derivatives of the perturbative energy are

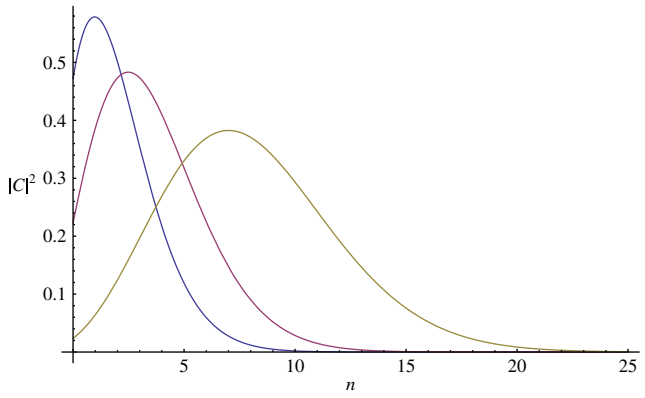

FIG. 9 (color online). The probability density $|c_n(J)|^2$ as a function of n. We set $\delta = 0.01$. Blue, purple, and gold lines correspond to $J = 3, 6, 15$.

[13]For simplicity, we choose $\gamma = 0$ in this section, so $\hat{\gamma} = \omega t$.

$$\epsilon_n^{\prime} = \hbar\omega\left[-3n\delta^2 + \left(1 - \frac{3}{2}\delta^2\right)\right] \qquad \epsilon_n^{\prime\prime} = -3\hbar\omega\delta^2. \tag{114}$$

Using $\tilde{n}$ and Eq. (114) allows us to determine the time scales involved,

$$T_{\mathrm{cl}} = 2\pi\hbar/|\epsilon_{\tilde{n}}^{\prime}| \approx \frac{2\pi}{\omega} + \frac{3\pi(2J+1)\delta^2}{\omega} \tag{115}$$

$$T_{\mathrm{rev}} = 4\pi\hbar/|\epsilon_{\tilde{n}}^{\prime\prime}| \approx \frac{4\pi}{3\omega\delta^2}. \tag{116}$$

Subsequently, we analyze the behavior of the autocorrelation function in order to study the revival structure. It is defined by the overlapping of states under the evolution of Hamiltonian,

$$A(t) := \langle J, \gamma | J, \gamma + t\omega\rangle = \sum_{n=0}^{n'} \frac{J^n e^{-it\omega\epsilon_n}}{N^2(J)\rho_n}. \tag{117}$$

One can choose an appropriate upper cutoff limit in the sum of Eq. (117) by analyzing the behavior of the square of weighting function $|c_n|^2$. For our situation as shown in Fig. 9, $n \approx 50$ will be a sufficiently good value to use as the termination point in the sum of the autocorrelation function.

Numerically, the square of the autocorrelation function $|A(t)|^2$ varies in between 0 and 1. The maximum $|A(t)|^2 = 1$ is the situation in which the wave packet $\psi(x,t) = \langle x|J, \omega t\rangle$ exactly matches the initial wave packet $\psi(x,0)$, whereas the minimum, $|A(t)|^2 = 0$, refers to nonoverlapping or the wave packet is far from the initial one. There will be a revival of the classical-like wave packet after the classical period T_{cl}. Since we have either sub-(super-) Poissonian distribution (depending on $\hat{\gamma}$) in our model, we also encounter the fractional revival as in the GUP stringy model [22]. The fractional revival occurs at time $p/q(T_{\mathrm{rev}})$, with coprime integers p, q. We show the revival

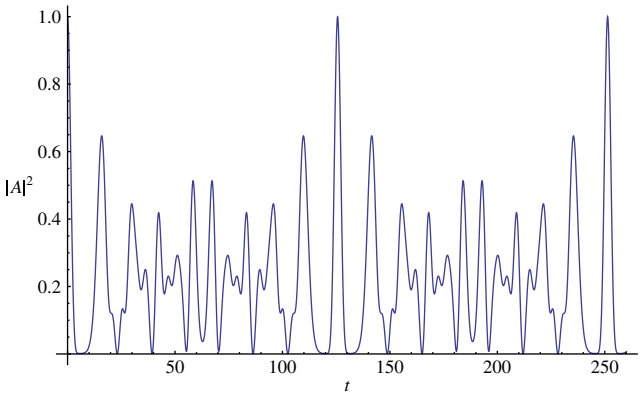

FIG. 10 (color online). Autocorrelation function as a function of time. We set $J = 1.5$, $\delta = 0.18$, $\omega = 0.5$, $\hbar = 1$, $\gamma = 0$, and $T_{\mathrm{cl}} = 15.08$, $T_{\mathrm{rev}} = 251.27$.

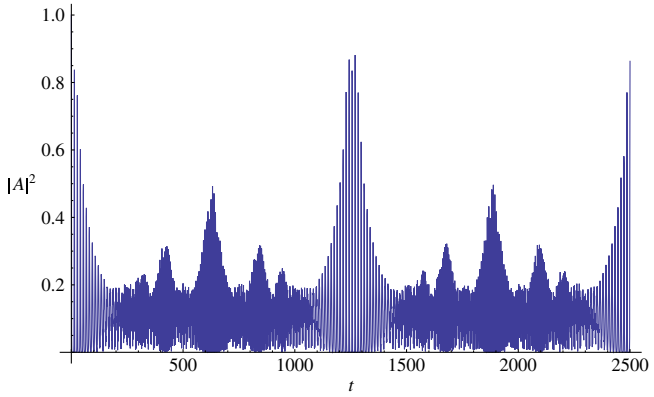

FIG. 11 (color online). Autocorrelation function as a function of time. We set $J = 6$, $\delta = 0.06$, $\omega = 0.5$, $\hbar = 1$, $\gamma = 0$, $T_{\mathrm{cl}} = 13.38$, and $T_{\mathrm{rev}} = 2513.27$.

structure in Figs. 10 and 11 for small (large) J values. In Fig. 10, we observe local maximum occurs at multiples of $T_{\mathrm{cl}} = 15.08$; i.e., $t = 15.08$, 30.16, 45.24, etc. Also, the first full reconstruction [18] of the original wave packet happens at $T_{\mathrm{rev}}/2 = 125.63$. In Fig. 11, we choose to set smaller δ so that the $T_{\mathrm{cl}} \ll T_{\mathrm{rev}}$ in order to observe the fractional revival structure clearly. The first reconstruction of the original wave occurs clearly at $T_{\mathrm{rev}} = 1256.64$. Furthermore, we see multiples of fractional revival occur at $T_{\mathrm{rev}}/4$, $T_{\mathrm{rev}}/3$, $T_{\mathrm{rev}}/6$, etc.

Note that our result in fractional revival is similar to Ref. [22] even though the latter case (stringy-motivated model) predicts strictly the sub-Poissonian distribution. Hence, we cannot distinguish the MCR and GUP models by investigating the autocorrelation function and the revival structure. The main reason is that we simplify the problem by using the perturbative approach. We believe the extension to higher orders or eventually the exact case will be able to determine the differences in the revival structure induced by these models.

VII. CONCLUSION

In this paper, we have successfully constructed GCSs that incorporate maximum momentum for $q = 1$ DHO exactly and obtained their probability distribution and entropy of states. However, the infinite potential box was studied perturbatively.

First, we review the bound state spectrum of both DHO and the infinite potential box. Their energies terminate at finite n level [14] and hence illustrate the main consequence of the DSR, which carries a maximum energy cutoff. Then, we review the generalized Heisenberg algebra scheme. This allow us to define the characteristic function and weight function of GCS. As an example, we consider the Planck length quantum optical system. We have computed exactly the probability density and entropy distribution as well as studied their behavior in terms of the

MCRs deformation. The entropy of the system increases in the presence of the maximum momentum in the model.

On the other hand, for simplicity, we have calculated the modified uncertainty principle perturbatively for $q = 1$ DHO. The GCSs constructed remain the squeezed type since they saturate the uncertainties $(\Delta X \Delta P)^{\mathrm{mup}}$, but with the minimal value shifted. The uncertainties may increase or decrease from the saturation point of the undeformed quantum optics depending on the value of γ. For $\gamma > 0$, it is possible that the MUP will at finite (J, γ) and hence exhibits the classical characteristics. This classical phase is generally different in nature compared to the DHO in Ref. [14].

Mandel's Q parameter has shown that the usual quantum description of laser light above threshold should be modified and behave as a sub-(super-)Poisonnian distribution. We have studied the motion of the center of the wave packet under the MCR. The Ehrenfest and correspondence principle are reproduced. Last, we have analyzed the autocorrelation function and obtained the quantum revival structure. Although the revival structure result is similar to the stringy model up to the first-order perturbation in $O(\delta)$, we believe the distinction should appear when higher-order perturbation or exact calculation is considered.

Overall, the GCS can be treated as an interesting model to distinguish the physics between the string theory motivated model, i.e., Snyder model, and the DSR-motivated $q = 1$ MCR model.

ACKNOWLEDGMENTS

C. L. C. would like to thank Dr. Parwani for great and stimulating discussions. He appreciates the kindness of P. Pedram for introducing his work on the GCS. Finally, we thank the referees for the valuable and critical comments.

APPENDIX

We present the computational scheme in detail here. Note that the expansions are performed up to $O(\delta)$ consistently. Recall the perturbed number state (80) is expressed as

$$|n\rangle = |n^{(0)}\rangle + i\frac{\delta}{\sqrt{8}}\Big[\Big(-\frac{1}{3}\Big)\Big(\sqrt{(n+1)_3}|n^{(0)}+3\rangle + \sqrt{(n-2)_2}|n^{(0)}-3\rangle\Big) + 3\Big(\sqrt{(n+1)_3}|n^{(0)}+1\rangle + \sqrt{(n)_3}|n^{(0)}-1\rangle\Big)\Big],$$

and thus

$$\langle m|A|n\rangle = \sqrt{n}\delta_{m,n-1} + i\frac{\delta}{\sqrt{8}}\Big[-\sqrt{(n+1)(n+2)}\delta_{m,n+2} + 3\Big((2n+1)\delta_{m,n} + \sqrt{n(n-1)}\delta_{m,n-2}\Big)\Big]. \tag{A1}$$

The expectation value of the annihilation operator is given by

$$\begin{aligned}\langle J,\gamma|A|J,\gamma\rangle &= \frac{1}{N^2(J)}\sum_{n,m}^{\infty}\frac{J^{(n+m)/2}e^{i\gamma(\epsilon_m-\epsilon_n)}}{\sqrt{\rho_m\rho_n}}\langle m|A|n\rangle \\ &= \frac{1}{N^2(J)}\sum_{n}^{\infty}\frac{\sqrt{n}J^{n-1/2}e^{i\gamma(\epsilon_{n-1}-\epsilon_n)}}{\rho_{n-1}\sqrt{\epsilon_m}} + i\frac{\delta}{\sqrt{8}}\Big\{\sum_{n}^{\infty}\frac{-\sqrt{(n+1)(n+2)}J^{n+1}e^{i\gamma(\epsilon_{n+2}-\epsilon_n)}}{N^2(J)\rho_n\sqrt{\epsilon_{n+2}\epsilon_{n+1}}} \\ &\quad + 3\sum_{n}^{\infty}\Big[\frac{(2n+1)J^n}{N^2(J)\rho_n} + \frac{\sqrt{n(n-1)}J^{n-1}e^{i\gamma(\epsilon_{n-2}-\epsilon_n)}}{N^2(J)\rho_{n-2}\sqrt{\epsilon_n\epsilon_{n-1}}}\Big]\Big\}.\end{aligned} \tag{A2}$$

We evaluate terms in Eq. (A2) individually. By using $\epsilon_{n-1} - \epsilon_n = -1 + 3n\delta^2$, the first term can be evaluated as

$$\begin{aligned}\frac{e^{-i\gamma}}{\sqrt{J}N^2(J)}\sum_{n}^{\infty}\frac{\sqrt{n}J^n e^{i3n\delta^2\gamma}}{\sqrt{\rho_{(n-1)}\rho_n}}|\text{use }\epsilon_n &= n[1-3(n+1)\delta^2/2] \\ &= \frac{e^{-i\gamma}}{\sqrt{J}N^2(J)}\sum_{n}^{\infty}\frac{J^n e^{i3n\delta^2\gamma}}{\rho_{(n-1)}\sqrt{1-3(n+1)\delta^2/2}} \\ &\approx \frac{e^{-i\gamma}}{\sqrt{J}N^2(J)}\Big[\sum_{n}^{\infty}\frac{(1+\frac{3\delta^2}{4})J^n}{\rho_{(n-1)}} + \sum_{n}^{\infty}\frac{(\frac{3}{4}+3i\gamma)\delta^2 nJ^n}{\rho_{(n-1)}}\Big] \\ &= \frac{e^{-i\gamma}}{\sqrt{J}}\Big[\Big(1+\frac{3\delta^2}{4}\Big)J + \Big(\frac{3}{4}+3i\gamma\Big)\delta^2 J\Big(1-\frac{2J}{3\delta^2}\cdot\frac{{}_0\tilde{\mathbf{F}}_1(3-\frac{2}{3\delta^2},-\frac{2J}{3\delta^2})}{{}_0\tilde{\mathbf{F}}_1(2-\frac{2}{3\delta^2},-\frac{2J}{3\delta^2})}\Big)\Big],\end{aligned}$$

where the regularized confluent hypergeometric function is given by ${}_0\tilde{\mathbf{F}}_1(a,x) = \frac{{}_0\mathbf{F}_1(a,x)}{\Gamma(a)}$. It is also related to the Bessel function of the first kind $J_\nu(x)$ by ${}_0\tilde{\mathbf{F}}_1(a,x) = (-x)^{(1-a)/2}J_{a-1}(a\sqrt{-x})$. For small δ, we see that we have the negative index for ${}_0\tilde{\mathbf{F}}_1(a,x)$.

We have the following ratio of the special function:

$$\frac{{}_0\tilde{\mathbf{F}}_1(3-\frac{2}{3\delta^2},-\frac{2J}{3\delta^2})}{{}_0\tilde{\mathbf{F}}_1(2-\frac{2}{3\delta^2},-\frac{2J}{3\delta^2})}=\frac{(\frac{2J}{3\delta^2})^{\frac{1-[3-\frac{2}{3\delta^2}]}{2}}J_{(3-\frac{2}{3\delta^2})-1}\left(2\sqrt{\frac{J}{3\delta^2}}\right)}{(\frac{2J}{3\delta^2})^{\frac{1-[2-\frac{2}{3\delta^2}]}{2}}J_{(2-\frac{2}{3\delta^2})-1}\left(2\sqrt{\frac{J}{3\delta^2}}\right)}=\sqrt{\frac{3\delta^2}{2J}}\left[\frac{J_{-(\frac{2}{3\delta^2}-\frac{5}{2}+\frac{1}{2})}\left(2\sqrt{\frac{J}{3\delta^2}}\right)}{J_{-(\frac{2}{3\delta^2}-\frac{3}{2}+\frac{1}{2})}\left(2\sqrt{\frac{J}{3\delta^2}}\right)}\right]\Bigg|\text{ let } n_2=2/(3\delta^2)-5/2;n_1=2/(3\delta^2)-3/2.$$

$$=\sqrt{\frac{3\delta^2}{2J}}\left[\frac{J_{-(n_2+\frac{1}{2})}\left(2\sqrt{\frac{J}{3\delta^2}}\right)}{J_{-(n_1+\frac{1}{2})}\left(2\sqrt{\frac{J}{3\delta^2}}\right)}\right]\Bigg|\text{ use identity } J_{-(n+1/2)}(z)=(-1)^{n+1}Y_{n+1/2}(z).$$

$$=-\sqrt{\frac{3\delta^2}{2J}}\left[\frac{Y_{(n_2+\frac{1}{2})}\left(2\sqrt{\frac{J}{3\delta^2}}\right)}{Y_{(n_1+\frac{1}{2})}\left(2\sqrt{\frac{J}{3\delta^2}}\right)}\right]\Bigg|\text{ use identity } Y_\nu(x)=\sim-\sqrt{\frac{2}{\pi\nu}}\left(\frac{ex}{2\nu}\right)^{-\nu};\nu\gg 0.$$

$$=-\sqrt{\frac{3\delta^2}{2J}}\sqrt{\frac{\frac{2}{3\delta^2}-\frac{3}{2}}{\frac{2}{3\delta^2}-\frac{5}{2}}}\left[\frac{\left(\frac{e\sqrt{2J/(3\delta^2)}}{\frac{2}{3\delta^2}-\frac{3}{2}}\right)^{\frac{2}{3\delta^2}-\frac{3}{2}}}{\left(\frac{e\sqrt{2J/(3\delta^2)}}{\frac{2}{3\delta^2}-\frac{5}{2}}\right)^{\frac{2}{3\delta^2}-\frac{5}{2}}}\right]$$

$$=-\frac{3\delta^2}{2}\left[1+\frac{15}{4}\delta^2+O(\delta^4)\right]. \tag{A3}$$

So, we have the first term in Eq. (A2):

$$\frac{e^{-i\gamma}}{\sqrt{J}N^2(J)}\sum_n^\infty\frac{\sqrt{n}J^n e^{i3n\delta^2\gamma}}{\sqrt{\rho_{(n-1)}\rho_n}}=e^{-i\gamma}\sqrt{J}\left[1+\frac{3}{4}\delta^2((J+2)+4i\gamma(J+1))\right]. \tag{A4}$$

The perturbed terms can be calculated as

$$\text{T 2: }\sum_n^\infty\frac{-\sqrt{(n+1)(n+2)}J^{n+1}e^{i\gamma(\epsilon_{n+2}-\epsilon_n)}}{N^2(J)\rho_n\sqrt{\epsilon_{n+2}\epsilon_{n+1}}}=-e^{2i\gamma}\sum_n^\infty\frac{J^{n+1}}{N^2(J)\rho_n}=-Je^{2i\gamma}; \tag{A5}$$

$$\text{T 3: }\sum_n^\infty\frac{(2n+1)J^n}{N^2(J)\rho_n}=2J+1 \tag{A6}$$

$$\text{T 4: }\sum_n^\infty\frac{\sqrt{n(n-1)}J^{n-1}e^{i\gamma(\epsilon_{n-2}-\epsilon_n)}}{N^2(J)\rho_{n-2}\sqrt{\epsilon_n\epsilon_{n-1}}}=e^{-2i\gamma}\sum_n^\infty\frac{J^{n-1}}{N^2(J)\rho_{n-2}}=Je^{-2i\gamma}. \tag{A7}$$

Thus, we have the expectation value of annihilation operator A up to $O(\delta)$ as

$$\langle J,\gamma|A|J,\gamma\rangle=\sqrt{J}e^{-i\gamma}-\frac{i\delta}{\sqrt{8}}[Je^{2i\gamma}-3(Je^{-2i\gamma}+2J+1)]. \tag{A8}$$

Note that we also have the following useful identities in order to evaluate the rest of expectation values:

$$\frac{{}_0\tilde{\mathbf{F}}_1(4-\frac{2}{3\delta^2},-\frac{2J}{3\delta^2})}{{}_0\tilde{\mathbf{F}}_1(2-\frac{2}{3\delta^2},-\frac{2J}{3\delta^2})}=\frac{9\delta^2}{4}[1+9\delta^2+O(\delta^4)]; \tag{A9}$$

$$\frac{J_{(3-\frac{2}{3\delta^2})}\left(2\sqrt{\frac{J}{3\delta^2}}\right)}{J_{(1-\frac{2}{3\delta^2})}\left(2\sqrt{\frac{J}{3\delta^2}}\right)}=\frac{3J}{2}\delta^2[1+9\delta^2+O(\delta^4)]; \tag{A10}$$

$$\frac{J_{(2-\frac{2}{3\delta^2})}\left(2\sqrt{\frac{J}{3\delta^2}}\right)}{J_{(1-\frac{2}{3\delta^2})}\left(2\sqrt{\frac{J}{3\delta^2}}\right)}=-\sqrt{\frac{3J}{2}}\delta\left[1+\frac{15}{4}\delta^2+O(\delta^4)\right]. \tag{A11}$$

Hence, all the expectation of the combination of creation/annihilation operators is given by

$$
\begin{aligned}
\langle J,\gamma|A^\dagger|J,\gamma\rangle &= \sqrt{J}e^{i\gamma} + \frac{i\delta}{\sqrt{8}}[Je^{-2i\gamma} - 3(Je^{2i\gamma} + 2J + 1)].\\
\langle J,\gamma|A^2|J,\gamma\rangle &= Je^{-2i\gamma} - \frac{2i\delta\sqrt{J}}{\sqrt{8}}[(J+1)(e^{i\gamma} - 6e^{-i\gamma}) - 3Je^{-3i\gamma}].\\
\langle J,\gamma|(A^\dagger)^2|J,\gamma\rangle &= Je^{2i\gamma} + \frac{2i\delta\sqrt{J}}{\sqrt{8}}[(J+1)(e^{-i\gamma} - 6e^{i\gamma}) - 3Je^{3i\gamma}].\\
\langle J,\gamma|A^\dagger A|J,\gamma\rangle &= J + \delta\sqrt{\frac{J}{2}}[J\sin 3\gamma - 3(J+1)\sin\gamma].\\
\langle J,\gamma|(A^\dagger)^2A^2|J,\gamma\rangle &= J^2 + \delta\sqrt{2J^3}[(J+1)\sin 3\gamma - 3(J+2)\sin\gamma].\\
\langle J,\gamma|A^3|J,\gamma\rangle &= J^{3/2}e^{-3i\gamma} - \frac{i\delta}{\sqrt{8}}[3J^2 + 2(3J+1) - 27(2J+3)e^{-2i\gamma} + 9J^2e^{-4i\gamma}].\\
\langle J,\gamma|(A^\dagger)^3|J,\gamma\rangle &= J^{3/2}e^{3i\gamma} + \frac{i\delta}{\sqrt{8}}[3J^2 + 2(3J+1) - 27(2J+3)e^{2i\gamma} + 9J^2e^{4i\gamma}].\\
\langle J,\gamma|A^\dagger A^2|J,\gamma\rangle &= J^{3/2}e^{-i\gamma} + \frac{i\delta J}{\sqrt{8}}[Je^{-4i\gamma} - 12(J+1)e^{2i\gamma} - 3e^{-2i\gamma} + 3(3J+4)].\\
\langle J,\gamma|(A^\dagger)^2A|J,\gamma\rangle &= J^{3/2}e^{i\gamma} - \frac{i\delta J}{\sqrt{8}}[Je^{4i\gamma} - 12(J+1)e^{-2i\gamma} - 3e^{2i\gamma} + 3(3J+4)].
\end{aligned}
\tag{A12}
$$

We can use these fundamental expectation values to compute the uncertainties in Sec. VI and the equation of motion of wave packet under the MCR in Secs. VI and II.

[1] A. Kempf, G. Mangano, and R. B. Mann, Phys. Rev. D **52**, 1108 (1995); A. Kempf, J. Phys. A **30**, 2093 (1997).
[2] H. S. Snyder, Phys. Rev. **71**, 38 (1947).
[3] L. N. Chang, D. Minic, N. Okamura, and T. Takeuchi, Phys. Rev. D **65**, 125028 (2002); Z. Lewis and T. Takeuchi, Phys. Rev. D **84**, 105029 (2011); L. N. Chang, Z. Lewis, D. Minic, and T. Takeuchi, Adv. High Energy Phys. **2011**, 493514 (2011); C. Quesne and V. M. Tkachuk, Phys. Rev. A **81**, 012106 (2010).
[4] F. Brau, J. Phys. A **32**, 7691 (1999); S. Das and E. C. Vagenas, Phys. Rev. Lett. **101**, 221301 (2008); K. Nozari and P. Pedram, Europhys. Lett. **92**, 50013 (2010); D. Bouaziz and N. Ferkous, Phys. Rev. A **82**, 022105 (2010); U. Harbach, S. Hossenfelder, M. Bleicher, and H. Stocker, Phys. Lett. B **584**, 109 (2004); M. Kober, Phys. Rev. D **82**, 085017 (2010); S. Ghosh and P. Roy, Phys. Lett. B **711**, 423 (2012); P. Pedram, J. Phys. A **45**, 505304 (2012).
[5] S. Hossenfelder, Living Rev. Relativity **16**, 2 (2013).
[6] I. Pikovski, M. R. Vanner, M. Aspelmeyer, M. Kim, and C. Brukner, Nat. Phys. **8**, 393 (2012).
[7] J. Magueijo and L. Smolin, Phys. Rev. Lett. **88**, 190403 (2002); Phys. Rev. D **67**, 044017 (2003); J. L. Cortes and J. Gamboa, Phys. Rev. D **71**, 065015 (2005); G. Amelino-Camelia, Phys. Lett. B **510**, 255 (2001).
[8] A. F. Ali, S. Das, and E. C. Vagenas, Phys. Lett. B **678**, 497 (2009); Phys. Rev. D **84**, 044013 (2011).
[9] S. Das, E. C. Vagenas, and A. F. Ali, Phys. Lett. B **690**, 407 (2010); P. Pedram, Phys. Lett. B **702**, 295 (2011).
[10] S. Mignemi, Phys. Rev. D **84**, 025021 (2011).
[11] P. Jizba, H. Kleinert, and F. Scardigli, Phys. Rev. D **81**, 084030 (2010).
[12] M. Maggiore, Phys. Lett. B **319**, 83 (1993); M. V. Battisti, Phys. Rev. D **79**, 083506 (2009).
[13] P. Pedram, Phys. Lett. B **714**, 317 (2012); **718**, 638 (2012).
[14] C. L. Ching, R. Parwani, and K. Singh, Phys. Rev. D **86**, 084053 (2012).
[15] C. L. Ching and R. R. Parwani, arXiv:1207.1519; Mod. Phys. Lett. A **28**, 1350061 (2013).
[16] C. L. Ching and W. K. Ng (to be published).
[17] C. Quesne and N. Vansteenkiste, J. Phys. A **28**, 7019 (1995); E. M. F. Curado and M. A. Rego-Monteiro, J. Phys. A **34**, 3253 (2001); Y. Hassouni, E. M. F. Curado, and M. A. Rego-Monteiro, Phys. Rev. A **71**, 022104 (2005).
[18] J.-P. Antoine, J.-P. Gazeau, P. Monceau, J. R. Klauder, and K. A. Penson, J. Math. Phys. (N.Y.) **42**, 2349 (2001).
[19] J. R. Klauder, J. Math. Phys. (N.Y.) **4**, 1055 (1963); Ann. Phys. (Amsterdam) **237**, 147 (1995); J. R. Klauder and J.-P. Gazeau, J. Phys. A **32**, 123 (1999); J. R. Klauder and B. S. Skagertan, *Coherent States: Applications in Physics and Mathematical Physics* (World Scientific, Singapore, 1985).
[20] P. Pedram, Int. J. Mod. Phys. D **22**, 1350004 (2013).
[21] S. Ghosh and P. Roy, Phys. Lett. B **711**, 423 (2012).
[22] S. Dey and A. Fring, Phys. Rev. D **86**, 064038 (2012).

[23] C. M. Bender and S. A. Orszag, *Advanced Mathematical Methods for Scientists and Engineers* (Springer, New York, 1999).
[24] E. Schrodinger, Naturwissenschaften **14**, 664 (1926).
[25] W.-M. Zhang, D. H. Feng, and R. Gilmore, Rev. Mod. Phys. **62**, 867 (1990); G. S. Agarwal and J. Benerji, Phys. Rev. A **64**, 023815 (2001); C. Quesne, J. Phys. A **35**, 9213 (2002).
[26] V. G. Drinfeld, in *Proceedings of the International Congress of Mathematicians, Berkeley, California, 1986* (American Mathematical Society, Providence, RI, 1987), p. 798.
[27] M. O. Scully and M. S. Zubairy, *Quantum Optics* (Cambridge University Press, Cambridge, England, 1997); L. Mandel and E. Wolf, *Optical Coherence and Quantum Optics* (Cambridge University Press, Cambridge, England, 1995).
[28] R. K. Pathria, *Statistical Mechanics* (Butterworth Heinemann, Oxford, London, 1996).